Accepted Manuscript

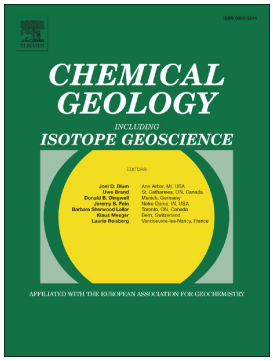

Hydrothermal dedolomitisation of carbonate rocks of the Paleoproterozoic Zaonega Formation, NW Russia — Implications for the preservation of primary C isotope signals

T. Kreitsmann, M. Külaviir, A. Lepland, K. Paiste, P. Paiste, A.R. Prave, H. Sepp, A.E. Romashkin, D.V. Rychanchik, K. Kirsimäe

PII: S0009-2541(19)30100-7
DOI: https://doi.org/10.1016/j.chemgeo.2019.03.002
Reference: CHEMGE 19091

To appear in: *Chemical Geology*

Received date: 26 October 2018
Revised date: 26 February 2019
Accepted date: 2 March 2019

Please cite this article as: T. Kreitsmann, M. Külaviir, A. Lepland, et al., Hydrothermal dedolomitisation of carbonate rocks of the Paleoproterozoic Zaonega Formation, NW Russia — Implications for the preservation of primary C isotope signals, Chemical Geology, https://doi.org/10.1016/j.chemgeo.2019.03.002

Hydrothermal dedolomitisation of carbonate rocks of the Paleoproterozoic Zaonega Formation, NW Russia — implications for the preservation of primary C isotope signals

T. Kreitsmann[1,*], M. Külaviir[1], A. Lepland[1,2,3], K. Paiste[2], P. Paiste[1], A. R. Prave[4], H. Sepp[1], A. E. Romashkin[5], D. V. Rychanchik[5], K. Kirsimäe[1]

[1]Department of Geology, University of Tartu, 50411 Tartu, Estonia.

[2]CAGE—Centre for Arctic Gas Hydrate, Environment and Climate, Department of Geosciences, UiT The Arctic University of Norway, 9037 Tromsø, Norway.

[3]Geological Survey of Norway (NGU), 7491 Trondheim, Norway.

[4]School of Earth and Environmental Sciences, University of St Andrews, St Andrews, KY16 9AL Scotland/UK.

[5]Institute of Geology, Karelian Science Centre, Pushkinskaya 11, 185610 Petrozavodsk, Russia.

*Corresponding author: email timmu.kreitsmann@ut.ee

Abstract

The Paleoproterozoic Zaonega Formation in Karelia, NW Russia, has played a key role in understanding the environmental conditions postdating the Great Oxidation and Lomagundi-Jatuli Events. Its carbonate- and organic-rich rocks (shungite) define the postulated Shunga Event representing an accumulation of very organic-rich sediments at c. 2 Ga and are central in ideas about changing ocean-atmosphere composition in the wake of those worldwide biogeochemical phenomena. Our work focussed on a key interval of carbonate rocks in the upper part of the Formation to: (i) obtain new high-resolution carbon, oxygen and strontium isotope data complemented by detailed petrography and mineralogical characterisation and (ii) expand upon previous studies by using our data to constrain geochemical modelling and show in greater detail how magmatic hydrothermal fluids induced dedolomitisation and altered geochemical signals. Our findings show that the $\delta^{13}C_{carb}$ of calcite-rich intervals are the most altered, with values between -16.9 to 0.6‰, whereas the dolomite-dominated parts retain the best-preserved (i.e. most original) values. Those define a trend of steadily

increasing $\delta^{13}C_{carb}$, from -6 to +0.5‰, which we interpret as a return to normal marine conditions and carbonate-carbon values following the Lomagundi-Jatuli Event.

Keywords: dedolomitisation, carbonate geochemistry, carbonate stable isotopes, Shunga Event

1. Introduction

The 4-billion-year-long record of the carbon cycle obtained from carbon isotopes of carbonate rocks and organic matter displays a remarkable trend: throughout most of Earth history it is typified by low-amplitude oscillations centering around 0.5‰ and -27‰, respectively (Schidlowski, 2001), reflecting an overall balance between carbon sources and sinks and carbon isotope fractionation between reduced and oxidised carbon. However, several large deviations (excursions), often attributed to global-scale perturbations of the C cycle (e.g., Kaufman and Knoll, 1995; Holland, 2004), punctuate that pattern. One of the largest was the 2.22-2.06 Ga Lomagundi-Jatuli Event, which is marked by $\delta^{13}C_{carb}$ (VPDB) values of as high as 15‰ (Karhu and Holland, 1996; Bekker and Holland, 2012). This perturbation was followed by the Shunga Event, an accumulation of extremely organic-rich sediments (C_{org} content > 10 wt%; Asael et al., 2013; Kump et al., 2011; Melezhik et al., 1999; Préat et al., 2011). Efforts to attain deeper understanding of these phenomena are rooted in the use of stable isotope data that are commonly interpreted as preserving signals obtained in equilibrium with contemporaneous seawater and largely being unchanged since deposition. It is therefore crucial to determine if such signals are actually syndepositional or, instead, record variable amounts of overprinting by later, post-depositional processes.

The carbonate- and organic-carbon isotope data from the Zaonega Formation, which occurs in the upper part of the Paleoproterozoic succession in the Onega Basin of NW Russia (Fig. 1), have played a central role in interpretations of the functioning of the carbon cycle during the Lomagundi-Jatuli and Shunga Events (Kump et al., 2011; Lyons et al., 2014; Melezhik et al., 1999). However, those rocks have experienced complicated diagenetic and metamorphic overprinting and obtaining geochemical proxies that preserve original (i.e. depositional) signals requires careful, detailed assessment of the origin of the minerals hosting those proxies (e.g., Črne et al., 2014; Paiste et al., 2018). Here we provide new high-resolution C,

O, and Sr isotope data combined with detailed mineralogy and petrography for a key interval of carbonate rocks in the upper part of the Zaonega Formation. We integrate these complementary data with mass-balance modelling of the host-rocks and secondary fluids. Our goal is to better constrain the effects of hydrothermal dedolomitisation on geochemical proxies and identify primary and secondary carbonate phases to better understand the extent of alteration. Further, ascertain the isotope values that best reflect original conditions gives us deeper insights into the C cycle during deposition of these strata.

2. Geological background

The Zaonega Formation is part of a thick Paleoproterozoic volcanic-sedimentary succession in the Onega Basin of NW Russia (Fig. 2). The Formation is sandwiched between the Tulomozero Formation, which preserves the c. 2.06 Ga Lomagundi-Jatuli Event (Karhu and Holland, 1996; Karhu, 2005; Melezhik et al., 2007), and the c. 1.98 Ga mafic lavas of the Suisari Formation (Puchtel et al., 1999, 1998). The entire Basin experienced greenschist-facies metamorphism during the 1.89-1.79 Ga Svecofennian orogeny (Melezhik et al., 2013). These age constraints suggest that the age of the Zaonega Formation is c. 2.0 Ga but more recent geochronology by Martin et al. (2015) suggests a younger age, between 1975.3 ±2.8 and 1967.6 ±3.5 Ma. Consequently, pending further geochronology, we adopt a conservative estimate of 1980 Ma as the age of the Zaonega Formation.

The Zaonega Formation is c. 1.5 km thick and consists of shallow to deeper marine mudstone, organic-rich mudstone, massive and bedded dolostone, limestone and contemporaneous mafic tuffs, lavas and sills, many of which have peperitic contacts indicative of intrusion into wet sediment (Črne et al., 2013, 2014). Deposition of the sedimentary layers occurred primarily by turbidity-current and background hemipelagic sedimentation (Melezhik et al., 2015). Associated with the igneous activity was widespread hydrothermal circulation, as evident from extensive silicification and silica veining in carbonate rocks (Črne et al., 2013, 2014). The Zaonega Formation is also one of the world's oldest and largest accumulations of organic carbon. Concentrations of C_{org} are commonly c. 25% but can reach 98% in pyrobitumen veins (Melezhik et al., 1999). Values of $\delta^{13}C_{org}$ are highly variable, between -45‰ to -17‰ (Melezhik et al., 1999; Qu et al., 2012). The genesis of strongly ^{13}C-depleted organic matter ($\delta^{13}C_{org}$ < -30‰, mostly in the upper part of the Formation) has been attributed variably to methanotrophic biomass (Lepland et al., 2014; Qu

et al., 2012; 2018), a global-scale oxidation of organic matter (Kump et al., 2011) and a biogeochemical response to the collapse of the global marine sulphate pool (Scott et al., 2014). Thus, better understanding of the geochemical and isotopic signals preserved in the carbonate rocks in the Zaonega Formation carries great significance for assessing the fluctuations of atmospheric oxygen concentration during Paleoproterozoic.

2.1 Previous geochemical studies

The Zaonega Formation has, over the past two decades, undergone much study and numerous workers have shown that carbonate rocks in the lower part of the Formation have strongly positive $\delta^{13}C_{carb}$ values, from +5 to +10‰, and that these decline to values as low as -25‰ in the upper part (Črne et al., 2014; Krupenik et al., 2011; Kump et al., 2011; Melezhik et al., 1999, 2015). This has led to the interpretation that the transition from the ^{13}C-rich carbonates to those with values near 0‰ in the middle part of the Formation denotes the end of the Lomagundi-Jatuli Event (Melezhik et al., 2015). The ^{13}C-depleted carbonate rocks in the upper part of the Formation were originally interpreted as concretions (Kuznetsov et al., 2012; Melezhik et al., 1999) but more recent studies have shown that they are variably altered sedimentary layers (Črne et al., 2014; Melezhik et al., 2015). Interpretations of such low $\delta^{13}C_{carb}$ values are quite variable and include: incorporation of C derived from anaerobic methane oxidation (Yudovich et al., 1991), diagenetic recrystallisation and incorporation of C derived from oxidised organic matter (Krupenik et al., 2011), and recycling of organic matter involving microbial and/or thermal reduction of sulphates and Fe- and Mn-oxides (Melezhik et al., 2015). However, the careful petrography and mineralogic work of Črne et al. (2014) documented intra-bed-scale variation of $\delta^{13}C_{carb}$ values as much as 17‰ and showed conclusively that isotopic signals are a function of the specific carbonate phase sampled: late-diagenetic to metamorphic calcite is significantly depleted in ^{13}C, via incorporation of C derived from diagenetic-catagenetic alteration of organic matter and possibly volcanic CO_2, whereas primary/early diagenetic dolomite preserves the least-altered values. Further, Fallick et al. (2016) documented a linear decrease in calcite $\delta^{18}O$ values with depth in the Zaonega Formation, which they interpreted as due to late-stage calcite that post-dated regional metamorphism and formed under near-surface geothermal gradients.

Other geochemical data from the Zaonega Formation, particularly the upper part, have also yielded varying interpretations regarding the timing and style of the early oxygenation of

Earth's surface environments. Based on Fe speciation and Mo, U and Se isotopes, dominantly euxinic water column conditions have been inferred (Asael et al., 2013, 2018; Kipp et al., 2017; Scott et al., 2014). In contrast, Re concentrations imply oxic conditions (Sheen et al., 2018) and the multiple S isotope data of Paiste et al. (2018) indicate that euxinia was not pervasive and that redox conditions in the basin may indeed have been episodically oxic.

3. Material and methods

Samples in this study were obtained from the Onega Parametric Hole (OPH) drilled 3.5 km deep in the southwest part (62.5870 N, 34.9310 E) of the Onega Basin (Fig. 1) in 2008–2009 (Glushanin et al., 2011). We focussed on four distinct carbonate intervals occurring within a 20 m section in the upper part of the Zaonega Formation at depths of 1103.62–1106.84, 1107.66–1111.99, 1115.43–1117.41 and 1122.33–1123.18 m; we label these beds A, B, C, and D. Microdrilling, using a 3-mm diameter drill bit, was used for obtaining material. Sample spacing was at 2 and 5-cm intervals inward from both the lower and upper bed contacts and increased to 10-cm spacing in the interior parts of the beds (Fig. 3B). In total, 116 microdrilled samples were collected. Additionally, 14 carbonate rock slabs were cut for microscopic analysis. All samples were targeted for mineralogical, carbon, and oxygen isotope analyses done at the University of Tartu, Estonia.

The mineralogical compositions of whole rock samples were studied by X-ray diffractometry (XRD). Unoriented preparations were made and scanned on a Bruker D8 Advance diffractometer using Cu *K*α radiation and LynxEye positive sensitive detector in 2–70° 2Θ range. Quantitative mineralogical composition was interpreted and modelled using the Rietveld algorithm-based program Topaz. The relative error of quantification is better than 10% for major phases (> 5 wt%) and better than 20% for minor phases (< 5 wt%).

Stable isotope ratios of O and C on bulk carbonate samples were measured on a Thermo Scientific Delta V Advantage continuous flow isotope ratio mass spectrometer with 0.2‰ precision (2σ). Long term reproducibility was better than ±0.2‰ (2σ) for $\delta^{18}O$ and $\delta^{13}C$. The results of carbonate mineral analyses are expressed in per mil deviation relative to the Vienna PeeDee Belemnite (VPDB) scale for oxygen and carbon. The $\delta^{18}O$ values are corrected for phosphoric acid fractionation factor for calcite and dolomite (Rosenbaum and Sheppard, 1986) in accordance with the mineralogy of individual samples.

Carbon isotope composition of bulk organic carbon was measured in the same powders used for carbonate isotope analysis and were reacted overnight with 10% HCl to remove carbonate phases. The retained material was rinsed multiple times with deionised water, dried and weighed for analysis with a Delta V Plus mass-spectrometer with Flash HT Plus interface. The C_{org} isotope composition is reported in per mil respective to VPDB.

Six samples with calcite and dolomite content varying from 1.2 to 69 wt% and 0.4 to 93.6 wt%, respectively, were selected for sequential dissolution experiments to assess the isotopic composition of calcite and dolomite end-members (*sensu* Al-Aasm et al., 1990). Sequential dissolution protocol of Al-Aasm et al. (1990) used a 2-hour reaction time at 25 °C in 99% phosphoric acid for calcite and 4 hours for dolomite at 50 °C. However, our XRD analysis on residues showed that, if the reaction time in the first step was longer than 30 minutes, significant amount of dolomite (> 10%) was dissolved along with complete removal of calcite. Reducing the reaction time to c. 20 minutes at 25 °C resulted in complete removal of calcite and only minor dissolution of dolomite (< 10%), hence we adopted this shorter reaction time for the first step. After CO_2 from the first step was retracted, the reaction vials were purged with He and the samples left to react overnight (8 hours) at 70 °C in the next step. Isotope values obtained from the first and second steps were assigned to calcite and dolomite, respectively.

Nineteen samples with varying dolomite and calcite ratio were chosen for strontium isotope and trace element analysis. The homogenised samples were leached in ultrapure 1M HCl for 1 hour at room temperature. Trace element concentrations were determined using an Agilent 8800 ICP-MS/MS with indium as the internal standard and NIST 1643f as the quality control standard. The Sr-isotope composition was measured on an Agilent 8800 ICP-MS/MS in double mass selection (MS/MS) mode using 10% of SF_6 in 90% He as the reaction gas in the Collision Reaction Cell. Signals were collected using 5 replicate measurements with 100 sweeps per replicate and 100 ms dwell times for $^{86,87,88}SrF^+$. Use of SF_6 reaction gas removes the spectral overlap from Rb, as the latter does not react with the gas (Cheng et al., 2008; Hogmalm et al., 2017). The Sr isotopic ratios are then measured at mass-to-charge ratios corresponding to SrF^+ ions, enabling accurate determination of the $^{87}Sr/^{86}Sr$ isotope ratio without prior Rb/Sr separation (Bolea-Fernandez et al., 2015). External correction was applied using NIST SRM 987 in a sample-standard bracketing protocol. USGS MACS-3, digested alongside the samples, was used as quality control standard for $^{87}Sr/^{86}Sr$ ratio measurements (average $^{87}Sr/^{86}Sr$ 0.7077 ± 0.0006). Initial $^{87}Sr/^{86}Sr$ values were calculated

and corrected for Rb using the equation by Banner (1995) with a decay constant λ_{87} = 1.3972 ± 0.0045 · 10^{-11} a^{-1} (Villa et al., 2015) given the geological age of 1.98 Ga. Corrected $^{87}Sr/^{86}Sr$ ratios were 0.01% – 1.31% lower than the measured values.

Carbon-coated thin sections and polished slabs were studied using a ZEISS EVO MA15 scanning electron microscope (SEM). The SEM images were captured in backscattered electron (BSE) mode and chemical characterisation by elemental mapping was carried out with an Oxford AZTEC-MAX energy dispersive spectroscopy detector (EDS) attached to the SEM.

To assess the variation of the isotope composition of carbonate rocks numerical modelling for closed (Eq 1) and open (Eq 2) systems was done (Jacobsen and Kaufman, 1999).

$$\delta_i^r(\eta) = \frac{\left(\frac{C_i^{ro}}{C_i^{wo}}\right)\delta_i^{r0} + \eta\,(\delta_i^{wo} + \Delta_i)}{\eta + \left(\frac{C_i^{ro}}{C_i^{wo}}\right)} \qquad \text{Eq (1)}$$

$$\delta_i^r(\eta) = \frac{\left(\frac{C_i^{ro}}{C_i^{wo}}\right)\delta_i^{r0} + D_i\left[exp\left(\frac{\eta}{D_i}\right) - 1\right][\Delta_i + \delta_i^{wo}]}{\left\{\left(\frac{C_i^{ro}}{C_i^{wo}}\right) + D_i\left[exp\left(\frac{\eta}{D_i}\right) - 1\right]\right\}} \qquad \text{Eq (2)}$$

Where δ_i^r is the final isotopic composition, η the weight ratio of fluid to rock, C_i^{ro} and C_i^{wo} the initial concentration of element *i* in the rock and fluid, respectively, D_i the effective rock-fluid distribution coefficient, Δ_i the fluid-rock isotope exchange fractionation factor for element *i* and δ_i^{wo} the initial isotopic composition of the fluid. The temperature of the system (given in Kelvin) is included in the Δ_i value, where the relationship between Δ_i and temperature (T) for calcite precipitation in the case of oxygen is expressed with Equation 3 (Friedman and O'Neil, 1977):

$$1000 ln\Delta_i = 2.78 \times 10^6 \times T^{-2} - 2.89 \qquad \text{Eq (3)}$$

4. Results

4.1. Petrography and mineralogy

The four carbonate beds are interlayered with organic-rich mudstones and intersected by silica and calcite veins. Whole-rock mineral composition of the analysed samples is shown in Figure 4 and in Supplementary Table 1. Mineral composition of the carbonate rocks is dominated by dolomite and calcite, varying from < 0.5 wt% (hereafter noted as trace amounts) to 93.6 wt% of crystalline phases and from 1.1 to 83.0 wt%, respectively. Calcite is the dominant carbonate phase on the margins of the beds whereas dolomite content is the highest in the interior parts of beds (Fig. 4). Margins of the beds are defined as the bottom- and top-most parts of the individual carbonate. Interiors represent the middle part of the carbonate beds. There is a clear negative co-variation between dolomite and calcite (Fig. 4).

Quartz (up to 52.7 wt%) and mica (up to 86.7 wt%) typically correlate with calcite, with higher abundances on the margins of the carbonate beds. Talc was identified in three carbonate beds (A, B, C) and its content can be as much as 15.8 wt%. Talc typically occurs in samples with higher calcite content, except carbonate bed D (depth of 1122.33–1123.18 m; Fig. 4). Carbonate-fluorapatite is a common accessory mineral (up to 6.1 wt%, average 0.9 wt%) found in all four beds. Pyrite content varies from trace amounts to 10.8 wt%, but its content is markedly higher in beds C and D (Fig. 4).

Dolomite most commonly exhibits planar-e (euhedral) (Fig. 5A and B) or intergrown planar-s (subhedral) rhombohedral (Fig. 5C) crystals mostly less than 150 µm in diameter. Size distribution of dolomite crystals is unimodal. Intra-crystalline calcite is common in dolomite crystals and can vary from a couple of µm in size (Fig. 5A) to large (> 100 µm) patches of either equicrystalline anhedral calcite filling the pore space between dolomite rhombohedral crystals (Fig. 5B and F) or as pseudomorphic replacement of dolomite (Fig. 6B). Dolomite crystals tend to have cloudier cores and clearer rims that can be enriched in Fe compared to the interior of the crystals (Fig. 6A). There is no correlation between iron enrichment in dolomite and stratigraphic position and Fe-rich dolomite occurs sporadically in all four carbonate beds. Pore space between dolomite crystals is mostly filled by anhedral calcite and talc near bed margins, whereas organic matter and mica fill the pore space in the interior part of the beds. Dolomite crystals occurring at the bed margins and next to the secondary veins can be larger and more recrystallised. Quartz can be found as massive anhedral aggregates, which are more common near the bed margins and filling secondary veins. Mica is mostly a

biotite-type phlogopite and occurs in trace amount throughout the carbonate beds but is more abundant at bed margins as a terrigenous input. Veins can be composed of quartz, phlogopite, talc, calcite and/or pyrobitumen. Phlogopite is texturally earlier than talc, as the latter occupies the pore space between phlogopite and dolomite (Fig. 5D, 6B).

4.2. Carbon, O, and Sr isotope composition

Carbon and oxygen stable isotope composition of the carbonate beds is shown in Figure 7 and in Supplementary Table 2. The first order trends are similar in all four beds: all show lower $\delta^{13}C_{carb}$ and $\delta^{18}O_{carb}$ (hereafter $\delta^{18}O$) values on the margins relative to bed interiors. Values of $\delta^{13}C_{carb}$ vary between -16.9 to 0.6‰. The highest values within interiors can vary by as much as 5‰ between individual carbonate beds. However, the $\delta^{13}C_{carb}$ values become consistently lower towards the margins, with minimum values reaching -16.9‰. There is also a compositional variability: dolomite-rich (defined as carbonate rocks with calcite/total carbonate ratio < 0.1) samples yield $\delta^{13}C_{carb}$ values between -9.5‰ and 0.6‰, whereas calcite-rich (defined as carbonate rock with calcite/total carbonate ratio > 0.8) samples have values between -16.9 and -7.1‰ (Fig. 8A).

The $\delta^{18}O$ values show high variability and range from -16.3 to -4.8‰. The $\delta^{18}O$ values are higher in the middle parts of the beds and lower on the margins, but the $\delta^{18}O$ trends are less clear compared to $\delta^{13}C_{carb}$ trends (Fig. 7). In the calcite-rich samples the $\delta^{18}O$ values are between -15.1 and -16.3‰, whereas in the dolomite-rich samples the $\delta^{18}O$ values vary between -12.1 and -4.8‰ (Fig. 8B).

Sequential dissolution experiments show that CO_2 extracted during the first step (20 min and 25 °C) was depleted in ^{13}C and ^{18}O up to 5‰ and 3‰, respectively, compared to the CO_2 extracted during the 2nd step (8 h and 70 °C; Fig. 9; Supplementary Table 3). The largest difference was in the samples with almost equal amount of calcite and dolomite (1st extraction: $\delta^{13}C_{carb}$ = -9.5‰, $\delta^{18}O$ = -13.5‰ and 2nd extraction: $\delta^{13}C_{carb}$ = -4.4‰ and $\delta^{18}O$ = -10.7‰), whereas the samples that were dominated by one phase showed the smallest difference (1st extraction in dolomite-rich samples: $\delta^{13}C_{carb}$ = -5.2‰, $\delta^{18}O$ = -9.2‰ and 2nd extraction: $\delta^{13}C_{carb}$ = -4.8‰ and $\delta^{18}O$ = -9.0‰, and 1st extraction in calcite-rich samples: $\delta^{13}C_{carb}$ = -12.3‰, $\delta^{18}O$ = -15.2‰ and 2nd extraction: $\delta^{13}C_{carb}$ = -11.3‰ and $\delta^{18}O$ = -14.4‰; Fig. 9). The $\delta^{13}C_{carb}$ and $\delta^{18}O$ values of bulk samples were consistently between the values of the first (predominantly calcite) and the second extraction (dolomite). Given the minor

dissolution of dolomite during the 1st extraction step, we are unable to assess the calcite end-member isotope composition in mixed carbonate samples. Nevertheless, the 2nd extraction step should characterise closely the $\delta^{13}C_{carb}$ and $\delta^{18}O$ values of dolomite. The $\delta^{18}O$ values of dolomite exhibit a systematic decreasing trend with increasing calcite abundance whereas the difference with the calcite end-member in the same sample is in the range of 0.3 to 2.8‰. This could be explained by high-temperature disequilibrium between calcite-dolomite pairs (Sheppard and Schwarch, 1970). The $\delta^{13}C_{carb}$ values of dolomite, however, remain relatively stable and presumably unchanged until calcite abundance reaches c. 50% of total carbonate (Fig. 9); a decreasing trend of dolomite $\delta^{13}C_{carb}$ values is only developed in samples with >50% calcite. Such isotope trends of dolomite indicate O isotope resetting of all samples regardless of the extent of dedolomitisation and calcite/dolomite ratio, but resistance of C isotope to resetting until calcite/dolomite ratio reaches c. 50%. Overall, our sequential dissolution experiments show that the isotope composition of studied carbonates do not represent a simple two component mixing with calcite and dolomite having distinct $\delta^{13}C_{carb}$ and $\delta^{18}O$ values.

The $\delta^{13}C_{org}$ values of the organic matter in most of the carbonate beds are relatively stable around -35.0‰ ±2.5‰, with the lowest value yielding -37.5‰. However, a 1-metre-thick interval in carbonate bed A, at a depth of about 1105 m, shows a gradual increase in $\delta^{13}C_{org}$ to as high as -24.3‰. This interval with the highest $\delta^{13}C_{org}$ values (from -26.3 to -24.3‰) overlaps with the highest $\delta^{13}C_{carb}$ values (from -0.53 to +0.58‰) (Fig. 7).

Strontium concentration is elevated in calcite-rich samples, reaching a maximum of 319 ppm, and is lower in dolomite-rich samples, varying between 46–156 ppm (Fig. 10); it also covaries with the amount of siliciclastic components (mica, K-feldspar; not shown). Sr-isotope ratios are highly variable, with $^{87}Sr/^{86}Sr$ values between 0.7139 and 0.7192 in calcite-rich samples and between 0.7062 and 0.7108 in dolomite-rich samples (Fig. 10). Mn/Sr ratio of the analysed samples for Sr isotopes varies between 0.8-8.2 (Fig. 10C), with the higher values associated with dolomite-rich samples and the lower values with calcite-rich samples.

5. Discussion

Carbonate rocks are typically considered capable of retaining syndepositional $\delta^{13}C_{carb}$ values under diagenetic recrystallisation and low-grade metamorphism (Hood et al., 2018;

Schidlowski, 2001; Swart, 2015; Valley and O'Neil, 1984), whereas their oxygen isotopic composition is more prone to resetting (Banner and Hanson, 1990). However, in the presence of silicate minerals, metamorphic silicate-carbonate reactions can cause isotopic resetting through re-equilibration with metamorphic fluids and/or due to decarbonation reactions (Valley, 1986). Both the $\delta^{13}C_{carb}$ and $\delta^{18}O$ values can be significantly altered at relatively lower temperatures/pressure by meteoric diagenesis and diagenetic/hydrothermal dolomitisation (Swart, 2015). Thus, the isotopic composition of carbonate phases can be altered under a variety of conditions and the preserved $\delta^{13}C_{carb}$ values are controlled by the composition of the original sediment, fluid, fluid/rock ratio during alteration, porosity, isotope fractionation factors, distribution coefficients, and open-system versus closed-system behaviour (Banner and Hanson, 1990; Bishop et al., 2014; Zheng and Hoefs, 1993).

5.1. Secondary alteration in the Zaonega carbonate rocks

Calcite crystallisation in the Zaonega Formation (Črne et al., 2014) and to a lesser extent in the Tulomozero Formation (Brasier et al., 2011) has been interpreted to be predominantly controlled by metamorphic calcite ± talc paragenesis (Eq. 4). This mineral association commonly develops in dolomitic rocks that have been subjected to metamorphic silica alteration, whereas dolomite replacement by calcite is accompanied by degassing of both ^{13}C- and ^{18}O-enriched CO_2, relative to the remaining carbonate material (Črne et al., 2014; Valley, 1986).

$$6[Ca, Mg(CO_3)_2] + 8SiO_2 + 2H_2O \rightarrow Mg_6[Si_8O_{20}](OH)_4 + 6CaCO_3 + 6CO_2 \quad \text{Eq. (4)}$$

This process would predict, even in the case of open-system devolatilisation, isotopic depletion with respect to ^{18}O and ^{13}C of calcite of, at most, a few per mil (Valley, 1986). This is not sufficient to account for the observed isotopic composition of secondary calcite in the Zaonega Formation. Further, the decrease in C-O isotope values combined with the intensification of dedolomitisation and silicification going from the interior of carbonate beds outward to the bed margins indicates that alteration was governed by fluid-rock alteration along the lithological contacts. Fluid controlled dedolomitisation is the replacement of dolomite by calcite in the presence of a water solution with elevated Ca^{2+} activity (Ayora et

al., 1998). Dedolomitisation has been extensively studied in both diagenetic and hydrothermal systems in relation to aquifer hydrochemistry and paleohydrogeology, burial diagenesis and porosity development and, more recently, in the context of CO_2 geological storage in natural and artificial analogue systems (e.g., Choi et al., 2012; Prado-Pérez and Pérez del Villar, 2011). Fluid driven dedolomitisation requires the reacting fluid to have a low Mg^{2+}/Ca^{2+} ratio (i.e. undersaturated with respect to dolomite and oversaturated with respect to calcite) and be able to remove the liberated Mg^{2+} to maintain dolomite undersaturation (Ayora et al., 1998). Importantly, dedolomitisation is known to occur under a wide variety of conditions, from karst and shallow subsurface settings due to interaction with meteoric waters at relatively low temperatures (<50 °C) and CO_2 partial pressures (Flügel, 2010; Nader et al., 2008; Rameil, 2008; Vandeginste and John, 2012) to deep burial environments (Budai et al., 1984; Land and Prezbindowski, 1981; Schoenherr et al., 2018; Woo and Moore, 1996) and hydrothermal systems (e.g., Faust, 1949; Matsumoto et al., 1988; Stoessell et al., 1987), such as those envisaged for the Zaonega Formation. One of the most convincing features to identify dedolomitisation microscopically is the replacement of dolomite rhombohedrons by equicrystalline anhedral calcite (Schoenherr et al., 2018). Such textures are present in the Zaonega Formation (e.g., Fig. 5 and 6).

Given that dedolomitisation occurs along bed margins, most of the fluid movement was bed-parallel, focused at mudstone-carbonate lithological contacts. However, in places fluids were able to penetrate dolomite beds via fractures but this did not have significant effect on the wall-rock as evidenced by the mineralogical and isotopic data of the samples from the vicinity of the veins. The intensification of dedolomitisation at bed margins acted to reduce permeability (as documented, for example, in Permian Zechstein carbonate rocks; Schoenherr et al., 2018) thereby shielding the middle part of carbonate beds from pervasive alteration. Dedolomitisation was additionally hindered inside the carbonates beds due to the closed-system behaviour with smaller supply of Ca^{2+} and/or slower removal of liberated Mg. Decreasing fluid temperatures inward are also evident from petrographical features of dolomite-calcite aggregates in the carbonate beds of the Zaonega Formation: these change from calcite occurring as patchy dolomite replacement in bed interiors to pseudomorphic replacement along the bed margins. Such textures have been generated in hydrothermal dedolomitisation experiments (Stoessell et al., 1988) via calcite replacement of dolomite in the interior of dolomite crystals associated with crystal imperfections. The importance of imperfections in dolomite stoichiometry was also noted by Nader et al (2008) and

Vandeginste and John (2012) who emphasised an excess of Fe in dolomite as a conducive factor for dolomite crystals to be altered. The variable Fe content in the Zaonega Formation carbonate beds also closely resembles this replacement pattern.

5.2. Fluid composition and source

Fluid circulation responsible for dedolomitisation was likely triggered by contemporaneous magmatic activity when gabbroic bodies intruded into unconsolidated wet sediments (Črne et al., 2013; Melezhik et al., 1999). Hydrothermal fluids carrying Ca, Si and CO_2 (and possibly CH_4 due to thermal cracking of organic matter) would have been enriched in light carbon derived from the encasing organic-rich muds. Further, the elevated Ca^{2+} activity would have been amply available from the underlying Tulomozero Formation. The latter is replete with quartz- and dolomite-pseudomorphed Ca-sulphate laths and nodules (Brasier et al., 2011; Melezhik et al., 2015) and the remarkable suite of evaporites recovered in the OPH core that consist of halite and Mg-K-sulfate minerals, anhydrite and magnesite-mudstone (Blättler et al., 2018; Krupenik et al., 2011). Hydrothermal circulation affecting the Tulomozero Formation has been also suggested by Fallick et al. (2016) and Melezhik et al. (2015) and is further supported by the findings of halite and sylvite micro-inclusions in the organic-rich mudstones of the Zaonega Formation (Kulikova, 2013). Thus, it is possible that these Ca-sulphate deposits of the Tulomozero Formation supplied the Ca ions needed for fluid-driven calcite supersaturation and precipitation evidenced throughout the carbonate beds in the Zaonega Formation.

The carbon isotopic composition of carbonate minerals is mainly controlled by the isotopic composition of dissolved inorganic carbon (DIC), given that the isotopic fractionation between DIC and the carbonate precipitating in the system is small and kinetic effects are negligible (Frisia et al., 2011; Romanek et al., 1992). Sources of ^{13}C-depleted DIC in the Zaonega Formation could have included: (a) volcanic CO_2 with $\delta^{13}C$ value of around -5‰, (b) products of decomposition/oxidation of organic material with $\delta^{13}C_{org}$ values between -42 and -25‰ and (c) oxidation products of organic material catagenesis (organic acids, biogenic and/or thermogenic methane) with $\delta^{13}C$ ranging from -50 to -20‰ (Qu et al., 2012; Whiticar, 1999). It is evident, that volcanic CO_2 would not be sufficient to produce calcite with measured depleted $\delta^{13}C_{carb}$ values. Additionally, it is unlikely that the oxidation of CH_4, (e.g., through anaerobic oxidation of methane, AOM) was the sole source of DIC because none of

the obtained $\delta^{13}C_{carb}$ values in calcite-rich carbonates is lower than -17‰. Typical AOM derived carbonates show $\delta^{13}C_{carb}$ values well below -20‰ (e.g., Campbell, 2006). Thus, the most probable source of ^{13}C-depleted DIC used for calcite precipitation was organic matter that has gone through thermal and/or microbial oxidation. This isotopically light DIC would have mixed locally with the carbon derived from dissolution of host-rock carbonates resulting in the variation of $\delta^{13}C_{carb}$ observed in the most calcite-rich samples.

Strontium isotope ratios show a strong correlation between radiogenic ^{87}Sr and calcite content. In calcite-rich samples, $^{87}Sr/^{86}Sr$ ratio can reach as high as 0.7192 whereas in dolomite-rich samples the ratios are lower, 0.7066-0.7138, with the lowest values matching the previously published $^{87}Sr/^{86}Sr$ data by Kuznetsov et al. (2012) for the Zaonega Formation. These, however, are slightly higher than the minimum $^{87}Sr/^{86}Sr$ ratio of 0.7041 reported by Blättler (2018) from the evaporites of the Tulomozero Formation. The source of the fluids enriched in radiogenic Sr (compared to host dolostone) responsible for calcite precipitation remains speculative but it could have been derived from the Archean granitoid basement and/or reworking of siliciclastic sediments. Regardless, Sr-isotope data clearly indicate that dolomite-rich interiors of beds were far less influenced by fluidal alteration compared to bed margins.

5.3. Development of the carbon isotope system

The relationships between $\delta^{13}C_{carb}$ and $\delta^{18}O$ values in carbonate rocks are often used to assess the effect of post-depositional alteration and determine if the values represent those of the ancient marine inorganic carbon reservoir (Bishop et al., 2014; Derry, 2010; Knauth and Kennedy, 2009; Swart, 2015). Jacobsen and Kaufman (1999) have shown, using mass-balance modelling, that partial resetting of the oxygen isotopic system in carbonates due to fluid-rock interaction may result in a $\delta^{13}C_{carb}$ and $\delta^{18}O$ trend on an exponential-like declining curve. During near complete resetting $\delta^{18}O$ and $\delta^{13}C_{carb}$ eventually reach values that differ from fluid $\delta^{18}O$ and $\delta^{13}C$ values only by the fluid/rock fractionation factor (Banner and Hanson, 1990; Jacobsen and Kaufman, 1999). It is interesting that the variation of the isotopic composition in studied carbonates plots in $\delta^{18}O$ and $\delta^{13}C_{carb}$ space (Fig. 11) on a similar exponential-like declining curve as modelled by Jacobsen and Kaufman (1999) possibly pointing to a fluidal mechanism of the dedolomitisation. However, the Zaonega Formation has experienced greenschist metamorphism, thus it has to be considered that

observed isotopic signal could have been altered by later processes. This is in particularly the case when it comes to carbonate $\delta^{18}O$ values that are easily reset in diagenetic-to-metamorphic and hydrothermal processes (Swart, 2015). Such resetting is further exemplified by the results of sequential leaching experiment (see Fig. 9). Therefore, the $\delta^{18}O$ values of the Zaonega Formation carbonates do not reflect, most possibly, neither the depositional dolomite signal nor the dedolomitisation environment (see also Fallick et al., 2016). Nevertheless, given the conservative nature of isotopic composition of the carbon we adopted the open and closed-system model by Jacobsen and Kaufman (1999). This model assesses the host-rock (dolostone) progressive reaction with a fluid at increasing water-rock ratio driving dedolomitisation, and its influence on the carbon isotope composition of the primary dolomite and secondary calcite. The open-system model assumes that each fluid increment reacts with the rock until elemental and isotopic equilibrium is achieved before the next iteration, whereas in closed-system one batch of water reacts without further iterations (Banner and Hanson, 1990).

Given the geochemical, petrographic and mineralogical data for the dolomite-rich samples, we interpret the isotopic values and stratigraphic C-isotope trend of the interior portions of beds A, B and C, from -6‰ to values around +1‰, as recording the best-preserved signals, i.e. those closest to representing depositional values. Thus, to assess the nature of fluid-rock interactions, we used different host-rock $\delta^{13}C_{carb}$ values ranging between -6 and +1‰. Isotopic system of oxygen is described in the model as arbitrary assuming the highest measured $\delta^{18}O$ value of -4.8‰ as the closest to normal marine dolomite.

Sensitivity analysis (Fig. 12) indicates that the isotope composition of the C-system depends on the differences of isotopic ratios between the end-members and carbon concentration in the reacting fluid. Alteration temperature affects primarily the isotopic exchange in oxygen (i.e. higher temperature produces a more L-shape curve). The change in $\delta^{13}C$ of the initial fluid defines the endpoint of the model (i.e. isotopic composition of secondary calcite) in the $\delta^{13}C$ scale. A similar trend would be evident for isotopic composition of the oxygen. Concentration of carbon in the reacting fluids controls the curvature of the hyperbolic evolution paths and higher carbon concentrations in the fluids results in a less curved path.

The greatest uncertainties for the modelling (besides the O-isotope system and the alteration temperature, see below) are the $\delta^{13}C$ value and carbon concentration of the reacting fluid. If we assume that calcite-rich samples with the lowest $\delta^{13}C_{carb}$ values (-16.9 to -7.1‰) were

precipitated from a fluid-buffered system and represent the alteration end-member, then the $\delta^{13}C$ value of the DIC in the fluid would have been around -20‰. Such ^{13}C depleted composition of dissolved carbon points to a fluid containing oxidised organic material or methane. We rule out a low temperature meteoric fluid because, although they can carry very variable carbon isotopic compositions (-7 to +1‰; Lohmann, 1988) such fluids cannot explain the very low $\delta^{13}C$ values in calcite-rich samples. Carbon concentration in fluid determines how much fluid is needed and how fast the $\delta^{13}C$ values of secondary calcite change compared to the host-rock. Concentration of carbon (HCO_3^- as dominant species) in the reacting fluid was chosen between 100-10000 ppm (Fig. 12A). The lower value represents surface water in contact with carbonate rocks and the upper value a high-temperature hydrothermal and/or metamorphic fluid. The best match with the measured values is achieved when the carbon concentration in the fluid is set around 5000 ppm.

It is important to distinguish different environments when it comes to open- versus closed-system behaviour between the interior of the carbonate beds and in the vicinity of bed contacts with mudstone. In the interior of carbonate beds the fluid/rock ratio decreases and DIC pool is influenced both by external fluid and the DIC derived from dolomite dissolution. The isotope signal of dolomite becomes more prevalent moving towards interiors of the carbonate beds. Thus, the samples from the inner parts of carbonate beds with minimal dedolomitisation should be treated as closed-systems where equilibrium was achieved between the fluid and the host-rock. Contrastingly, the nearly completely dedolomitised margins with calcite characterised by the lowest $\delta^{13}C_{carb}$ values can be explained by open-system behaviour. Open-system reaction describes well the margins of carbonate beds where the water/rock ratio is high and the composition of the secondary calcite, and to the lesser extent dolomite, is mainly fluid-buffered. It is apparent from leaching experiments that C-isotope composition remains nearly unchanged in samples with calcite-dolomite ratio less than 0.5. Somewhat lower $\delta^{13}C_{carb}$ values and nearly complete resetting of $\delta^{18}O$ values of the dolomite end-member are apparent in samples with high calcite content. Hence, the modelled $\delta^{13}C_{carb}$ (and $\delta^{18}O$) values are mostly determined by the external fluid parameters.

In summary, our modelling results indicate that the best fit between the measured and modelled values can be achieved via interaction between the dolostone host-rock and a fluid with carbon concentration of 5000 ppm, $\delta^{13}C$ value of the fluid ranging -20 to -25‰, and $\delta^{18}O_{SMOW}$ values between +5‰ and +10‰ (values of typical hydrothermal fluid; Sheppard, 1986) at temperatures between 215 °C and 380 °C, respectively (Fig. 12). Further, the

water/rock ratio had to be high in order to achieve $\delta^{13}C_{carb}$ values as low as measured in calcite-rich samples. We stress, though, the fluid oxygen composition and temperature estimation should be taken with caution due to likely oxygen isotope resetting during the Svecofennian orogeny.

Noteworthy is that Fallick et al. (2016), who examined the O-isotope values and trend of the calcite-dominated carbonate rocks for the 400-m-thick Zaonega Formation, interpreted those as recording surface derived water-rock interaction under a geothermal gradient at near-surface conditions. However, our data indicate fluid temperatures between 215 – 380 °C that may refer either to dedolomitisation and/or greenschist environment, whether it be the temperature of metamorphic conditions or dedolomitisation.

5.4.Timing of the dedolomitisation

Placing the timing of dedolomitisation to hydrothermal circulation triggered by near syndepositional magmatic activity is supported by the lithological and textural evidence exhibited by the carbonate beds in the upper Zaonega Formation (e.g., Črne et al., 2013, 2014). Firstly, alteration is spatially localised to lithological contacts and does not extend into the interior of carbonate beds. Secondly, mafic igneous rocks comprise about half of the Formation. Many are tuffs and lavas, hence were undeniably contemporaneous with sedimentation. The numerous sills that cut the Formation have peperitic contacts that indicate intrusion into wet sediment not yet lithified. In such settings, magmatic bodies often initiate hydrothermal circulation. Thirdly, typical metamorphic dedolomitisation reactions and expected isotopic shifts are not capable of explaining the observed geochemical signals (calcite-rich samples with $\delta^{13}C_{carb}$ values of -17‰), which are, instead, compatible with processes driven by hydrothermal fluid alteration. Suggestions that dedolomitisation might be due to greenschist facies metamorphism of the Svecofennian Orogeny some 100 to 200 million of years after deposition are incompatible with our observations. Particularly, given the fact that such metamorphism is regional and thus affected all the rocks in the Onega Basin, it would not be restricted contacts of carbonate beds that occur in the upper Zaonega Formation.

We propose a dedolomitisation model (Fig. 13) that was triggered by hydrothermal fluids that circulated in the Zaonega Formation. Timing of fluid circulation would have been early enough that the mudstones were not yet lithified to act as conduits for fluid migration. Thus,

most of the dedolomitisation is observed on the contact zones of mudstones and carbonate beds (these would have been more lithified compared to mudstones). In order to trigger dedolomitisation the fluid had to be Ca^{2+}-rich and liberated Mg^{2+} removed to maintain dolomite undersaturation. We infer that the source for the high concentration of Ca^{2+} would be fluids that migrated upward from the underlying Tulomozero Formation, likely driven by hydrothermal circulation by the magmatic activity initiated during Zaonega time. Liberated Mg^{+2} could have been transported away if the water/rock ratio was high enough or incorporated into secondary talc, which our observation show is concentrated on the carbonate bed margins. This fluid also carried a DIC that was depleted in ^{13}C due to thermal and/or microbial oxidation of organic matter in the organic-rich mudstones of the Zaonega Formation. Dedolomitisation is only limited to the carbonate bed margins suggesting that migration to the middle parts of the carbonate beds were hindered. Replacement of dolomite with calcite is accompanied with decrease in porosity thereby limiting the supply of Ca^{+2} to initiate dedolomitisation. This also explains the gradual increase in isotopic values and dolomite/calcite ratios from the mudstone-dolostone contacts inward to carbonate bed interiors.

6. Implications to preservation of the depositional carbon isotope signal

The influence of secondary alteration on the isotopic values preserved in marine carbonate rocks depends significantly on the geological history of individual successions. Different geochemical proxies have been used to assess the extent of such alteration. One that has been widely used to discriminate between altered and least-altered dolostones in Proterozoic-Archean rocks is the Mn/Sr_{carb} ratio (Kaufman and Knoll, 1995), with ratios of <10 used as a metric to identify those most likely as preserving original signals. Interestingly, all of our samples of the Zaonega carbonate rocks in the OPH core have Mn/Sr_{carb} <10, yet all petrographic, mineralogical and geochemical observations show a clear influence of secondary alteration. Our explanation is that the low Mn/Sr ratios in calcite-rich samples reflect the addition of Sr that was leached from micas and feldspar that have higher concentration in calcite-rich samples compared to purer dolomite-rich samples. Additional Sr could have been also inherited from the underlying Tulomozero evaporites that are enriched in Sr compared to the dolomitic carbonate rocks of the upper Zaonega Formation. Noteworthy is that Črne et al. (2014) also documented that calcite is enriched in Sr compared

to dolomite in the uppermost carbonate bed in the correlative FAR-DEEP-13A drill core. Thus, in our samples Mn/Sr_{carb} ratio is not a reliable screening tool.

All of the geochemical and isotopic data reported above indicate that the dolomite-dominated middle section of the carbonate beds retain the best preserved, possibly primary, $\delta^{13}C_{carb}$ signals. Intermediate values reflect either the physical mixture of primary dolomite and secondary calcite and/or a rock-buffered closed-system alteration. We do acknowledge that bulk carbonate samples show mixtures of signals from calcite and dolomite. However, as can be observed on Figure 9, it only becomes relevant if there is approximately equal amount of both phases. Thus, knowing the mineralogy of the samples is key to distinguishing between these values. There is no evidence of a clearly hydrothermal dolomite (i.e. saddle dolomite) in the studied carbonate beds of the upper Zaonega Formation other than some larger recrystallised dolomite aggregates at the contacts with mudstones and secondary veins.

To summarise, the samples carrying the best preserved isotopic signal reside in the interiors of the carbonate beds. These portions of the beds typically have a total carbonate content of at least 90 wt% and calcite-to-total-carbonate ratio <0.1. For screening the best preserved dolomite total carbonate content was set to 90 wt% because dolomite at carbonate beds margins, where there is also higher concentration of terrigenous material, might have been partially reset its carbon isotopic signal (Fig. 9). Using this as a screening tool, 30 samples can be classified as best preserved, and all are from beds A to C. Screened samples show a lack of correlation between $\delta^{18}O$ and $\delta^{13}C_{carb}$ values (Fig. 14B), giving us additional confidence in our screening criteria. The resulting trend in $\delta^{13}C_{carb}$ values displays a rise from -6.3‰ in bed C to a surprisingly stable +0.4‰ in bed A (Fig. 14A). Note that, even though the $\delta^{13}C_{carb}$ value of -3.6‰ in bed D (which is less than 1 m thick) is compatible with the overall upward trend in $\delta^{13}C_{carb}$ defined by beds C through A, it does not pass the screening criteria and we do not use it in our summary compilation on Figure 14A.

Interestingly, the consistent $\delta^{13}C_{carb}$ values around 0‰ in the middle of bed A coincide with an abrupt change in $\delta^{13}C_{org}$ from -37.5 to -25‰ (Fig. 7). Given that organic matter with values of $\delta^{13}C_{org}$ < -25‰ could reflect methane cycling and methanotrophy, this change may represent conditions during a time of limited, if any, methane cycling, as also reflected in the near "normal" $\delta^{13}C_{carb}$ values. If so, then both the rather large variations in $\delta^{13}C_{carb}$ values displayed in the individual carbonate beds (as much as 4‰) and those as low as -6.3‰ might well indicate the varying influence of a fluctuating methanotrophic biomass and associated

variable flux of methanotrophic DIC to the seafloor and into the seawater DIC pool. Recently, (Qu et al., 2018) showed the presence of both methanotrophic and photoautotrophic biomass in the upper part of the Zaonega Formation, supporting this interpretation.

Previously published $\delta^{13}C_{carb}$ data from the OPH core (Krupenik et al., 2011) have not provided a detailed assessment of secondary alteration in the Zaonega carbonates. With our careful screening of the least-altered samples we can compare our data to that from FAR-DEEP 12AB and 13A drill-cores reported by Črne et al. (2014) and Melezhik et al. (2015). The base of our bed B, a massive dolostone bed with distinctive apatite nodules associated with organic-rich mudstone, occurs at 1112 m depth in the OPH core and at 9.25 m and 43.1 m depth in FAR-DEEP 12AB and 13A, respectively (for more details see Paiste el al., 2018). In all three cores, after screening for the least-altered samples, those stratigraphic positions also record a shift to heavier $\delta^{13}C_{carb}$ values, from -6 to -2‰ in the FAR-DEEP cores (Črne et al., 2014; Melezhik et al., 2015) and from -6‰ to +0.5‰ in our data from the OPH core. In summary, the trend defined by the least-altered carbonate rocks in the upper Zaonega Formation can be considered as representing the evolution of C-isotope composition in the Onega Basin and the establishment of "normal" marine conditions following the perturbations in the carbon cycle during the Lomagundi-Jatuli and Shunga Events.

7. Conclusion

The Zaonega Formation has figured prominently in paleoenvironmental interpretations of the conditions characterising Earth's surface following the Great Oxidation and Lomagundi-Jatuli Events and during the Shunga Event. With our expanded database of isotope geochemistry, underpinned by detailed petrography and mineralogy, we show that the only reliable archive of original signals in the Zaonega Formation are the dolostone interiors of carbonate beds. In contrast, the calcite-rich outer edges of carbonate beds carry a secondary hydrothermal dedolomitisation signal. We propose a dedolomitisation model that describes the secondary alteration in the Zaonega Formation and explains the mixed dolomite-calcite mineralogy. Further, our modelling supports the idea that the dedolomitisation process was driven by Ca-rich and ^{13}C-depleted hydrothermal fluids. Hydrothermal fluid, initiated by syndepositional magmatic activity, inherited Ca from the underlying Tulomozero Formation and DIC from the organic-rich rocks of the Zaonega Formation below the carbonate unit. Secondary calcite (dedolomite) is characterised by isotopically light stable isotope

composition, typically with $\delta^{18}O$ -16‰ and $\delta^{13}C_{carb}$ -17‰. The best-preserved carbonate rocks in the upper Zaonega Formation, the dolomite-rich middle section of carbonate beds, define an upward trend of increasing ^{13}C-enrichment from $\delta^{13}C_{carb}$ values of -6‰ to +0.5‰. We interpret this trend to represent an original signal that marks termination of the large-scale perturbations in the carbon cycle (e.g., the Lomagundi-Jatuli and Shunga Events) and a return to a normal marine conditions.

8. Acknowledgements

We are grateful to Alex Brasier, Tony Fallick, Johannes Schoenherr and one anonymous reviewer whose suggestions greatly improved the manuscript. This study was supported by Estonian Science Agency project PUT696 and PRG447, and Estonian Centre of Analytical Chemistry. K.P. and A.L. were supported by the Research Council of Norway through its Centres of Excellence funding scheme grant No. 223259.

Figure captions

Figure 1. Simplified geological map of the Onega basin (Koistinen et al., 2001) with location of the Onega Parametric Hole (OPH) and FAR-DEEP holes 12AB and 13A.

Figure 2. Simplified lithostratigraphic column of the Onega Parametric Hole showing the studied interval of the upper Zaonega Formation (carbonate beds A-D indicated).

Figure 3. Photos of drill core samples with sampling spots and obtained $\delta^{18}O$ and $\delta^{13}C_{carb}$ values in ‰ (VPDB). Red rectangles represent where thin sections were made. (A) Sample from 1105.2 m depth (bed A), notice the secondary calcite and bitumen veining. (B) Sample from 1123.03 m depth (bed D), the contact between the carbonate bed and underlying organic-rich mudstone. (C) and (D) samples from 1,109.42 (bed B) and 1104.31 m depths (bed A) respectively, highlighting brecciated areas with quartz, calcite and bitumen matrix.

Figure 4. Mineral composition of the studied carbonate beds (wt%). Letters in white circles show the location of the samples from Figure 3. See Figure 2 for lithostratigraphic legend.

Figure 5. SEM BSE images and EDS elemental maps of representative petrographical associations. (A) Sample from 1111.4 m depth, massive unimodal planar-e dolomite crystals

in organic matrix. (B) Sample from 1111.8 m depth, planar-e dolomite (dark-grey) with secondary calcite (dedolomites; light-grey) in organic matrix. (C, E) Sample from 1109.4 m depth, secondary calcite and quartz filling pore space and partially superimposed on planar-s dolomite crystals. Note the existence of quartz and absence of talc. (D, F) Sample from 1106.82 m depth, lower contact of carbonate bed A on mudstone. Note anhedral calcite, remnant dolomite cores and abundant talc. Abbreviations: Cal – calcite, Dol – dolomite, Org – organic matter, Q – quartz.

Figure 6. SEM BSE images (A) Sample from 1115.43 m depth highlighting the heterogeneity of dolomites. Lighter areas of dolomites are more Fe-rich compared to darker areas, also note the cloudier cores and small calcite inclusions in dolomite. (B) Sample from 1106.82 m depth, paragenesis of dedolomitisation; note the remnant dolomite core, secondary calcite and talc filling the pore space between dolomite and mica flakes.

Figure 7. Dolomite and calcite abundances along with $\delta^{13}C_{carb,}$ $\delta^{18}O_{carb}$, $\delta^{13}C_{org}$ (‰, VPDB), and $^{87}Sr/^{86}Sr$ ratio values. See Figure 2 for lithostratigraphic legend.

Figure 8. Cross-plot of calcite/total carbonate ratio (1 being pure calcite and 0 pure dolomite) and (a) $\delta^{13}C_{carb}$ (b) $\delta^{18}O_{carb}$ (VPDB). Note the overlapping $\delta^{13}C_{carb}$ values in dolomite and calcite-rich samples and limited range of $\delta^{18}O_{carb}$ values in calcite-rich samples.

Figure 9. Sequential dissolution of bulk samples with varying concentration of calcite and dolomite. First step lasted 20 min at 25 °C and second step took 24 h at 70 °C. Bulk samples were analysed using standard method as discussed in the text. The first extraction refers to calcite and the second extraction to dolomite end-member. Calcite end-member (i.e. 1st extraction) shows consistently lower $\delta^{13}C$ (A) and $\delta^{18}O$ (B) values than dolomite end-member (i.e. 2nd extraction). Oxygen isotope values have been reset in calcite and dolomite whereas inferred original carbon isotope values has retained in dolomite-rich samples.

Figure 10. Cross-plot of Sr isotope ratio and different geochemical parameters grouped by carbonate mineralogy. (A) Positive correlation between Sr concentration and $^{87}Sr/^{86}Sr$ ratio. (B) Negative correlation between $\delta^{13}C_{carb}$ and $^{87}Sr/^{86}Sr$ ratio. (C) Mn_{carb}/Sr_{carb} ratio is <10 in all samples, but higher in dolomite-rich samples. (D) Negative correlation between $\delta^{18}O$ and $^{87}Sr/^{86}Sr$ ratio.

Figure 11. Cross-plot of $\delta^{13}C_{carb}$ and $\delta^{18}O_{carb}$ values grouped by carbonate mineralogy.

Figure 12. Sensitivity analysis of the model with varying fluid parameters. Measured $\delta^{13}C$ and $\delta^{18}O$ values are plotted on the background. Solid lines show closed-system and dashed lines open-system behaviour. Dolostone host-rock $\delta^{18}O$ was set to 0‰ and $\delta^{13}C$ +1‰, -1‰, -3‰, -6‰. Fluid temperature was set 300 °C with $\delta^{18}O_{SMOW}$ = 7.7‰, $\delta^{13}C$ = -25‰, C_{carbon} = 5000. (ppm) unless noted otherwise. Plots show the effect of carbon concentration in the fluid (A) and $\delta^{13}C$ value of the fluid (B) on the precipitating phase. W/R stands for water-to-rock ratio.

Figure 13. Conceptual dedolomitisation model. (A) Describes the situation before the magmatic activity that initated hydrothermal alteration and (B) describes the fluid movement during dedolomitisation. Dashed white arrows indicate fluid circulation and movement that is concentrated in mudstones; these would have been unlithified whereas carbonate beds which would have been at least semi-lithified. The source of Ca^{2+} is the dissolution of evaporites in the underlying Tulomozero Formation that moved upward due to the hydrothermal circulation initiated by the magamatic activity during the Zaonega times. Magmatic activity also triggered the migration of organic matter (i.e. pyrobitumen veins and seafloor oilspills; Qu et al., 2012). Black lines are the faults that could have acted as conduits for the vertical fluid movement. Dark-blue outer edges of carbonate beds show the area of dedolomitisation. Dedolomites are depleted in $\delta^{18}O$ and $\delta^{13}C$ compared to the better preserved interiors of carbonate beds.

Figure 14. Plots of least-altered samples after screening; these samples had total carbonate concentration at least 90 wt% and calcite-to-total-carbonate ratio < 0.1. (A) Upward increasing $\delta^{13}C_{carb}$ trend to values around 0‰. (B) Cross-plot of $\delta^{13}C$ and $\delta^{18}O$ of least-altered samples; the lack of correlation gives us confidence that there has been no significant alteration.

Supplementary table captions

Supplementary table 1. Mineralogical composition of whole rock samples for the Onega Parametric Hole drill-core from the upper Zaonega Formation carbonate rocks.

Supplementary table 2. Oxygen, carbonate carbon, organic carbon isotope values, strontium isotope ratios, and carbonate manganese, strontium and rubidium concentrations for the Onega Parametric Hole drill-core from the upper Zaonega Formation carbonate rocks.

Supplementary table 3. Calcite and dolomite concentration and oxygen and carbonate carbon isotope values of the sequential dissolution experiment.

References

Al-Aasm, I.S., Taylor, B.E., South, B., 1990. Stable isotope analysis of multiple carbonate samples using selective acid extraction. Chemical Geology 80, 119–125. https://doi.org/10.1016/0168-9622(90)90020-D

Asael, D., Rouxel, O., Poulton, S.W., Lyons, T.W., Bekker, A., 2018. Molybdenum record from black shales indicates oscillating atmospheric oxygen levels in the early Paleoproterozoic. American Journal of Science 318, 275–299. https://doi.org/10.2475/03.2018.01

Asael, D., Tissot, F.L.H., Reinhard, C.T., Rouxel, O., Dauphas, N., Lyons, T.W., Ponzevera, E., Liorzou, C., Chéron, S., 2013. Coupled molybdenum, iron and uranium stable isotopes as oceanic paleoredox proxies during the Paleoproterozoic Shunga Event. Chemical Geology 362, 193–210. https://doi.org/10.1016/j.chemgeo.2013.08.003

Ayora, C., Taberner, C., Saaltink, M.W., Carrera, J., 1998. The genesis of dedolomites: a discusion based on reactive transport modeling. Journal of Hydrology 209, 346–365. https://doi.org/10.1016/S0022-1694(98)00095-X

Banner, J.L., 1995. Application of the trace element and isotope geochemistry of strontium to studies of carbonate diagenesis. Sedimentology 42, 805–824. https://doi.org/10.1111/j.1365-3091.1995.tb00410.x

Banner, J.L., Hanson, G.N., 1990. Calculation of simultaneous isotopic and trace element variations during water-rock interaction with applications to carbonate diagenesis. Geochimica et Cosmochimica Acta 54, 3123–3137. https://doi.org/10.1016/0016-7037(90)90128-8

Bekker, A., Holland, H.D., 2012. Oxygen overshoot and recovery during the early Paleoproterozoic. Earth and Planetary Science Letters 317–318, 295–304. https://doi.org/10.1016/j.epsl.2011.12.012

Bishop, J.W., Osleger, D.A., Montañez, I.P., Sumner, D.Y., 2014. Meteoric diagenesis and fluid-rock interaction in the Middle Permian Capitan backreef: Yates Formation, Slaughter Canyon, New Mexico. AAPG Bulletin 98, 1495–1519. https://doi.org/10.1306/05201311158

Blättler, C.L., Claire, M.W., Prave, A.R., Kirsimäe, K., Higgins, J.A., Medvedev, P.V., Romashkin, A.E., Rychanchik, D.V., Zerkle, A.L., Paiste, K., Kreitsmann, T., Millar, I.L., Hayles, J.A., Bao, H., Turchyn, A.V., Warke, M.R., Lepland, A., 2018. Two-billion-year-old evaporites capture Earth's great oxidation. Science 360, 320–323. https://doi.org/10.1126/science.aar2687

Bolea-Fernandez, E., Balcaen, L., Resano, M., Vanhaecke, F., 2015. Tandem ICP-mass spectrometry for Sr isotopic analysis without prior Rb/Sr separation. Journal of Analytical Atomic Spectrometry 31, 303–310. https://doi.org/10.1039/C5JA00157A

Brasier, A.T., Fallick, A.E., Prave, A.R., Melezhik, V.A., Lepland, A., 2011. Coastal sabkha dolomites and calcitised sulphates preserving the Lomagundi-Jatuli carbon isotope signal. Precambrian Research 189, 193–211. https://doi.org/10.1016/j.precamres.2011.05.011

Budai, J.M., Lohmann, K.C., Owen, R.M., 1984. Burial dedolomite in the Mississippian Madison Limestone, Wyoming and Utah thrust belt. Journal of Sedimentary Research 54, 276–288. https://doi.org/10.1306/212F83FF-2B24-11D7-8648000102C1865D

Campbell, K.A., 2006. Hydrocarbon seep and hydrothermal vent paleoenvironments and paleontology: Past developments and future research directions. Palaeogeography, Palaeoclimatology, Palaeoecology 232, 362–407. https://doi.org/10.1016/j.palaeo.2005.06.018

Cheng, P., Koyanagi, G.K., Bohme, D.K., 2008. On the chemical resolution of the ^{87}Rb+ (s0)/^{87}Sr+ (s1) isobaric interference: A kinetic search for an optimum reagent. Analytica Chimica Acta 627, 148–153. https://doi.org/10.1016/j.aca.2008.03.057

Choi, B.-Y., Yun, S.-T., Mayer, B., Hong, S.-Y., Kim, K.-H., Jo, H.-Y., 2012. Hydrogeochemical processes in clastic sedimentary rocks, South Korea: A natural analogue study of the role of dedolomitization in geologic carbon storage. Chemical Geology 306–307, 103–113. https://doi.org/10.1016/j.chemgeo.2012.03.002

Črne, A.E., Melezhik, V.A., Prave, A.R., Lepland, A., Romashkin, A.E., Rychanchik, D.V., Hanski, E.J., Luo, Z., 2013. Zaonega formation: FAR-DEEP hole 13A. In: Melezhik V. A., Prave A. R., Fallick A. E., Hanski E. J., Lepland A., Kump L. R., Strauss H. (Eds.), Reading the Archive of Earth's Oxygenation: Volume 2: The Core Archive of the Fennoscandian Arctic Russia - Drilling Early Earth Project. Springer, pp. 1008-1046. https://doi.org/10.1007/978-3-642-29659-8_4

Črne, A.E., Melezhik, V.A., Lepland, A., Fallick, A.E., Prave, A.R., Brasier, A.T., 2014. Petrography and geochemistry of carbonate rocks of the Paleoproterozoic Zaonega Formation, Russia: Documentation of ^{13}C-depleted non-primary calcite. Precambrian Research 240, 79–93. https://doi.org/10.1016/j.precamres.2013.10.005

Derry, L.A., 2010. A burial diagenesis origin for the Ediacaran Shuram–Wonoka carbon isotope anomaly. Earth and Planetary Science Letters 294, 152–162. https://doi.org/10.1016/j.epsl.2010.03.022

Fallick, A.E., Melezhik, V.A., Brasier, A.T., Prave, A.R., 2016. Unusual, basin-scale, fluid–rock interaction in the Palaeoproterozoic Onega basin from Fennoscandia: Preservation in calcite $\delta^{18}O$ of an ancient high geothermal gradient. Precambrian Res. 281, 224– 235. https://doi.org/10.1016/j.precamres.2016.06.001

Faust, G. T., 1949. Dedolomitization, and its relation to a possible derivation of a magnesium-rich hydrothermal solution*. American Mineralogist 34, 780-823.

Flügel, E., 2010. Microfacies of Carbonate Rocks: Analysis, Interpretation and Application, 2nd ed. Springer-Verlag, Berlin Heidelberg.

Friedman, I., O'Neil, J.R., 1977. Compilation of stable isotope fractionation factors of geochemical interest. U.S. Geological Survey Professional Paper 440 KK. https://doi.org/10.3133/pp440KK

Frisia, S., Fairchild, I.J., Fohlmeister, J., Miorandi, R., Spötl, C., Borsato, A., 2011. Carbon mass-balance modelling and carbon isotope exchange processes in dynamic caves. Geochimica et Cosmochimica Acta 75, 380–400. https://doi.org/10.1016/j.gca.2010.10.021

Glushanin, L.V., Sharov, N.V., Shchiptsov, V.V., 2011. The Onega palaeoproterozoic structure (geology, tectonics, deep structure and mineralogeny). Institute of Geology, Karelian Research Centre of RAS, Petrozavotsk, 431 pp (in Russian).

Hogmalm, K.J., Zack, T., Karlsson, A.K.O., Sjöqvist, A.S.L., Garbe-Schönberg, D., 2017. In situ Rb–Sr and K–Ca dating by LA-ICP-MS/MS: an evaluation of N_2O and SF_6 as reaction gases. Journal of Analytical Atomic Spectrometry 32, 305–313. https://doi.org/10.1039/C6JA00362A

Holland, H.D., 2004. The geologic history of seawater. In: Elderfield, H. (Ed.) The Oceans and Marine Chemistry. Elsevier, Amsterdam, pp.583-625.

Hood, A. v. S., Planavsky, N.J., Wallace, M.W., Wang, X., 2018. The effects of diagenesis on geochemical paleoredox proxies in sedimentary carbonates. Geochimica et Cosmochimica Acta 232, 265–287. https://doi.org/10.1016/j.gca.2018.04.022

Jacobsen, S.B., Kaufman, A.J., 1999. The Sr, C and O isotopic evolution of Neoproterozoic seawater. Chemical Geology 161, 37–57. https://doi.org/10.1016/S0009-2541(99)00080-7

Karhu, J.A., 2005. Paleoproterozoic carbon isotope excursion. In: Lehtinen, M., Nurmi, P.A., Rämö, O.T. (Eds.), Precambrian Geology of Finland: Key to the Evolution of the Fennoscandian Shield, Developments in Precambrian Geology. Elsevier Science B.V., The netherlands, pp. 669–680.

Karhu, J.A., Holland, H.D., 1996. Carbon isotopes and the rise of atmospheric oxygen. Geology 24, 867–870. https://doi.org/10.1130/0091-7613(1996)024<0867:CIATRO>2.3.CO;2

Kaufman, A.J., Knoll, A.H., 1995. Neoproterozoic variations in the C-isotopic composition of seawater: stratigraphic and biogeochemical implications. Precambrian Research 73, 27–49. https://doi.org/10.1016/0301-9268(94)00070-8

Kipp, M.A., Stüeken, E.E., Bekker, A., Buick, R., 2017. Selenium isotopes record extensive marine suboxia during the Great Oxidation Event. PNAS 114, 875–880. https://doi.org/10.1073/pnas.1615867114

Knauth, L.P., Kennedy, M.J., 2009. The late Precambrian greening of the Earth. Nature 460, 728–732. https://doi.org/10.1038/nature08213

Koistinen, T., Stephens, M.B., Bogatchev, V., Nordgulen, Ø., Wenneström, M., Korhonen, J., 2001. Geological Map of the Fennoscandian Shield. Scale 1:2,000,000. Geological Surveys of Finland, Norway and Sweden and the North-West Department of Natural Resources of Russia.

Krupenik V. A., Akhmedov A. M. and Sveshnikova K. Y. (2011) Isotopic composition of carbon, oxygen and sulfur in the Ludicovian and Jatulian rocks. In: Glushanin L. V., Sharov N. V., Shchiptsov V. V. (Eds.), The Onega Paleoproterozoic Structure (Geology, Tectonics, Deep Structure, Minerageny). Institute of Geology, Karelian Research Centre RAS, Petrozavodsk, 250-255 (in Russian).

Kulikova, V.V., 2013. Halite and sylvinite as chemical indicators of different-age basins (an example from C_{org}-bearing sediments – shungites from SE Fennoscandia). In: Vakulenko, L.G., Jan, P.A. (Eds), Sedimentary basins, sedimentary and post-sedimentary processes in geological history. Proceedings of the VII All-Russia Lithological Meeting, Novosibirsk, 28-31 October, 2013, 138-142 (in Russian).

Kump, L.R., Junium, C., Arthur, M.A., Brasier, A., Fallick, A., Melezhik, V., Lepland, A., Črne, A.E., Luo, G., 2011. Isotopic Evidence for Massive Oxidation of Organic Matter Following the Great Oxidation Event. Science 334, 1694–1696. https://doi.org/10.1126/science.1213999

Kuznetsov, A.B., Gorokhov, I.M., Melezhik, V.A., Mel'nikov, N.N., Konstantinova, G.V., Turchenko, T.L., 2012. Strontium isotope composition of the lower proterozoic

carbonate concretions: The Zaonega Formation, Southeast Karelia. Lithology and Mineral Resources 47, 319–333. https://doi.org/10.1134/S0024490212030066

Land, L.S., Prezbindowski, D.R., 1981. The origin and evolution of saline formation water, Lower Cretaceous carbonates, south-central Texas, U.S.A. Journal of Hydrology, Symposium on Geochemistry of Groundwater 54, 51–74. https://doi.org/10.1016/0022-1694(81)90152-9

Lepland, A., Joosu, L., Kirsimäe, K., Prave, A.R., Romashkin, A.E., Črne, A.E., Martin, A.P., Fallick, A.E., Somelar, P., Üpraus, K., Mänd, K., Roberts, N.M.W., Van, Z., Wirth, R., Schreiber, A., 2014. Potential influence of sulphur bacteria on Palaeoproterozoic phosphogenesis. Nature Geoscience 7, 20–24. https://doi.org/10.1038/ngeo2005

Lohmann, K.C., 1988. Geochemical patterns of meteoric diagenetic systems and their application to studies of paleokarst. In: James, N.P., Choquette, P.W. (Eds.), Paleokarst, Springer New York, pp. 58–80. https://doi.org/10.1007/978-1-4612-3748-8_3

Lyons, T.W., Reinhard, C.T., Planavsky, N.J., 2014. The rise of oxygen in Earth's early ocean and atmosphere. Nature 506, 307. https://doi.org/10.1038/nature13068

Martin, A.P., Prave, A.R., Condon, D.J., Lepland, A., Fallick, A.E., Romashkin, A.E., Medvedev, P.V., Rychanchik, D.V., 2015. Multiple Palaeoproterozoic carbon burial episodes and excursions. Earth and Planetary Science Letters 424, 226–236. https://doi.org/10.1016/j.epsl.2015.05.023

Matsumoto, R., Iijima, A., Katayama, T., 1988. Mixed-water and hydrothermal dolomitization of the Pliocene Shirahama Limestone, Izu Peninsula, central Japan. Sedimentology 35, 979–998. https://doi.org/10.1111/j.1365-3091.1988.tb01741.x

Melezhik, V.A., Fallick, A.E., Filippov, M.M., Larsen, O., 1999. Karelian shungite—an indication of 2.0-Ga-old metamorphosed oil-shale and generation of petroleum: geology, lithology and geochemistry. Earth-Science Reviews 47, 1–40. https://doi.org/10.1016/S0012-8252(99)00027-6

Melezhik, V.A., Huhma, H., Condon, D.J., Fallick, A.E., Whitehouse, M.J., 2007. Temporal constraints on the Paleoproterozoic Lomagundi-Jatuli carbon isotopic event. Geology 35, 655–658. https://doi.org/10.1130/G23764A.1

Melezhik V. A., Medvedev P. V. and Svetov S. A., 2013. The Onega Basin. In: Melezhik V. A., Prave A. R., Hanski E. J., Fallick A. E., Lepland A., Kump L. R., Strauss H. (Eds.), Reading the Archive of Earth's Oxygenation: Volume 1: The Paleoproterozoic of Fennoscandia as Context for the Fennoscandian Arctic Russia - Drilling Early Earth Project. Springer, 249-287.

Melezhik, V.A., Fallick, A.E., Brasier, A.T., Lepland, A., 2015. Carbonate deposition in the Palaeoproterozoic Onega basin from Fennoscandia: a spotlight on the transition from the Lomagundi-Jatuli to Shunga events. Earth-Science Reviews 147, 65–98. https://doi.org/10.1016/j.earscirev.2015.05.005

Nader, F.H., Swennen, R., Keppens, E., 2008. Calcitization/dedolomitization of Jurassic dolostones (Lebanon): results from petrographic and sequential geochemical analyses. Sedimentology 55, 1467–1485. https://doi.org/10.1111/j.1365-3091.2008.00953.x

Paiste, K., Lepland, A., Zerkle, A.L., Kirsimäe, K., Izon, G., Patel, N.K., McLean, F., Kreitsmann, T., Mänd, K., Bui, T.H., Romashkin, A.E., Rychanchik, D.V., Prave, A.R., 2018. Multiple sulphur isotope records tracking basinal and global processes in the 1.98 Ga Zaonega Formation, NW Russia. Chemical Geology 499, 151–164. https://doi.org/10.1016/j.chemgeo.2018.09.025

Prado-Pérez, A.J., Pérez del Villar, L., 2011. Dedolomitization as an analogue process for assessing the long-term behaviour of a CO_2 deep geological storage: The Alicún de las Torres thermal system (Betic Cordillera, Spain). Chemical Geology 289, 98–113. https://doi.org/10.1016/j.chemgeo.2011.07.017

Préat, A., Bouton, P., Thiéblemont, D., Prian, J.P., Ndounze, S.S., Delpomdor, F., 2011. Paleoproterozoic high $\delta^{13}C$ dolomites from the Lastoursville and Franceville basins (SE Gabon): Stratigraphic and synsedimentary subsidence implications. Precambrian Research 189, 212–228. https://doi.org/10.1016/j.precamres.2011.05.013

Puchtel, I.S., Arndt, N.T., Hofmann, A.W., Haase, K.M., Kröner, A., Kulikov, V.S., Kulikova, V.V., Garbe-Schönberg, C.-D., Nemchin, A.A., 1998. Petrology of mafic lavas within the Onega plateau, central Karelia: evidence for 2.0 Ga plume-related continental crustal growth in the Baltic Shield. Contributions to Mineralogy and Petrology 130, 134–153. https://doi.org/10.1007/s004100050355

Puchtel, I.S., Brügmann, G.E., Hofmann, A.W., 1999. Precise Re–Os mineral isochron and Pb–Nd–Os isotope systematics of a mafic–ultramafic sill in the 2.0 Ga Onega plateau (Baltic Shield). Earth and Planetary Science Letters 170, 447–461. https://doi.org/10.1016/S0012-821X(99)00118-1

Qu, Y., Črne, A.E., Lepland, A., van Zuilen, M.A., 2012. Methanotrophy in a Paleoproterozoic oil field ecosystem, Zaonega Formation, Karelia, Russia. Geobiology 10, 467–478. https://doi.org/10.1111/gbi.12007

Qu, Y., Lepland, A., van Zuilen, M.A., Whitehouse, M., Črne, A.E., Fallick, A.E., 2018. Sample-scale carbon isotopic variability and diverse biomass in the Paleoproterozoic Zaonega Formation, Russia. Precambrian Research 315, 222–231. https://doi.org/10.1016/j.precamres.2018.07.008

Rameil, N., 2008. Early diagenetic dolomitization and dedolomitization of Late Jurassic and earliest Cretaceous platform carbonates: A case study from the Jura Mountains (NW Switzerland, E France). Sedimentary Geology 212, 70–85. https://doi.org/10.1016/j.sedgeo.2008.10.004

Romanek, C.S., Grossman, E.L., Morse, J.W., 1992. Carbon isotopic fractionation in synthetic aragonite and calcite: Effects of temperature and precipitation rate. Geochimica et Cosmochimica Acta 56, 419–430. https://doi.org/10.1016/0016-7037(92)90142-6

Rosenbaum, J., Sheppard, S.M.F., 1986. An isotopic study of siderites, dolomites and ankerites at high temperatures. Geochimica et Cosmochimica Acta 50, 1147–1150. https://doi.org/10.1016/0016-7037(86)90396-0

Schidlowski, M., 2001. Carbon isotopes as biogeochemical recorders of life over 3.8 Ga of Earth history: evolution of a concept. Precambrian Research 106, 117–134. https://doi.org/10.1016/S0301-9268(00)00128-5

Schoenherr, J., Reuning, L., Hallenberger, M., Lüders, V., Lemmens, L., Biehl, B.C., Lewin, A., Leupold, M., Wimmers, K., Strohmenger, C.J., 2018. Dedolomitization: review and case study of uncommon mesogenetic formation conditions. Earth-Science Reviews 185, 780–805. https://doi.org/10.1016/j.earscirev.2018.07.005

Scott, C., Wing, B.A., Bekker, A., Planavsky, N.J., Medvedev, P., Bates, S.M., Yun, M., Lyons, T.W., 2014. Pyrite multiple-sulfur isotope evidence for rapid expansion and contraction of the early Paleoproterozoic seawater sulfate reservoir. Earth and Planetary Science Letters 389, 95–104. https://doi.org/10.1016/j.epsl.2013.12.010

Sheen, A.I., Kendall, B., Reinhard, C.T., Creaser, R.A., Lyons, T.W., Bekker, A., Poulton, S.W., Anbar, A.D., 2018. A model for the oceanic mass balance of rhenium and implications for the extent of Proterozoic ocean anoxia. Geochimica et Cosmochimica Acta 227, 75–95. https://doi.org/10.1016/j.gca.2018.01.036

Sheppard, S.M.F., Schwarcz, H.P., 1970. Fractionation of carbon and oxygen isotopes and magnesium between coexisting metamorphic calcite and dolomite. Contributions to Mineralogy and Petrology 26, 161-198. https://doi.org/10.1007/BF00373200

Sheppard, S.M.F., 1986. Characterization and isotopic variations in natural waters. Reviews in Mineralogy and Geochemistry 16, 165–183.

Stoessell, R.K., Klimentidis, R.E., Prezbindowski, D.R., 1987. Dedolomitization in Na□Ca□Cl brines from 100° to 200°C at 300 bars. Geochimica et Cosmochimica Acta 51, 847–855. https://doi.org/10.1016/0016-7037(87)90098-6

Swart, P.K., 2015. The geochemistry of carbonate diagenesis: The past, present and future. Sedimentology 62, 1233–1304. https://doi.org/10.1111/sed.12205

Valley, J.W., 1986. Stable isotope geochemistry of metamorphic rocks. Reviews in Mineralogy and Geochemistry 16, 445–489.

Valley, J.W., O'Neil, J.R., 1984. Fluid heterogeneity during granulite facies metamorphism in the Adirondacks: stable isotope evidence. Contributions to Mineralogy and Petrology. 85, 158–173. https://doi.org/10.1007/BF00371706

Vandeginste, V., John, C.M., 2012. Influence of climate and dolomite composition on dedolomitization: insights from a multi-proxy study in the central Oman Mountains. Journal of Sedimentary Research 82, 177–195. https://doi.org/10.2110/jsr.2012.19

Villa, I.M., De Bièvre, P., Holden, N.E., Renne, P.R., 2015. IUPAC-IUGS recommendation on the half life of 87Rb. Geochimica et Cosmochimica Acta 164, 382–385. https://doi.org/10.1016/j.gca.2015.05.025

Whiticar, M.J., 1999. Carbon and hydrogen isotope systematics of bacterial formation and oxidation of methane. Chemical Geology 161, 291–314. https://doi.org/10.1016/S0009-2541(99)00092-3

Woo, K.S., Moore, C.H., 1996. Burial dolomitization and dedolomitization of the late Cambrian Wagok Formation, Yeongweol, Korea. Carbonates Evaporites 11, 104–112. https://doi.org/10.1007/BF03175789

Yudovich, I.E., Makarikhin, V.V., Medvedev, P.V., Sukhanov, N.V., 1991. Carbon isotope anomalies in carbonates of the Karelian Complex. Geochemistry International 28, 56-62.

Zheng, Y.F., Hoefs, J., 1993. Carbon and oxygen isotopic covariations in hydrothermal calcites. Mineralium Deposita 28, 79–89. 79–89. https://doi.org/10.1007/BF00196332

Highlights:

- Carbonates of the Zaonega Formation have been influenced by the hydrothermal alteration
- Hydrothermal fluids were ^{13}C-depleted and Ca^{2+}-rich
- The dolomite-rich centres of carbonate beds are least affected by the secondary processes and carry the best preserved geochemical signal
- Best preserved $\delta^{13}Ccarb$ values show a shift from -6 to +0.5‰

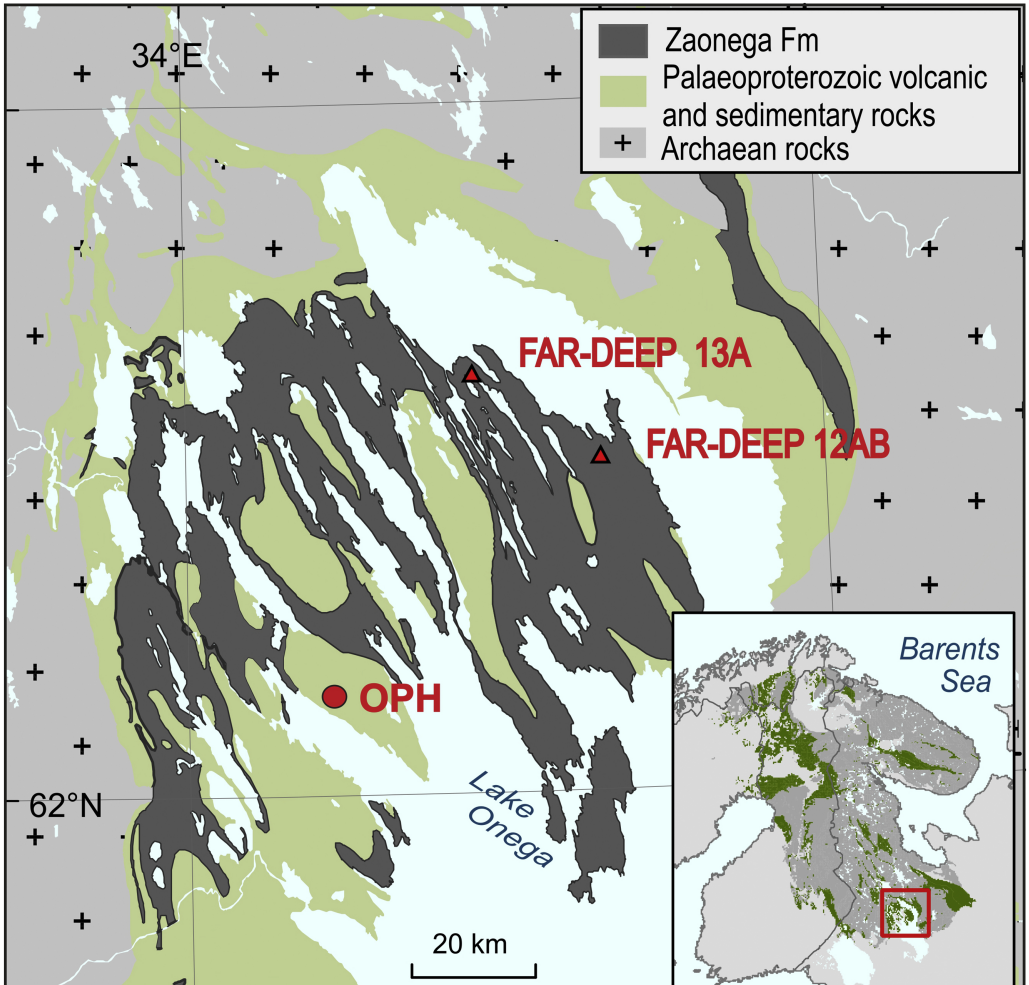
Zaonega Fm
Palaeoproterozoic volcanic and sedimentary rocks
Archaean rocks
34°E
62°N
FAR-DEEP 13A
FAR-DEEP 12AB
OPH
Lake Onega
20 km
Barents Sea

Figure 1

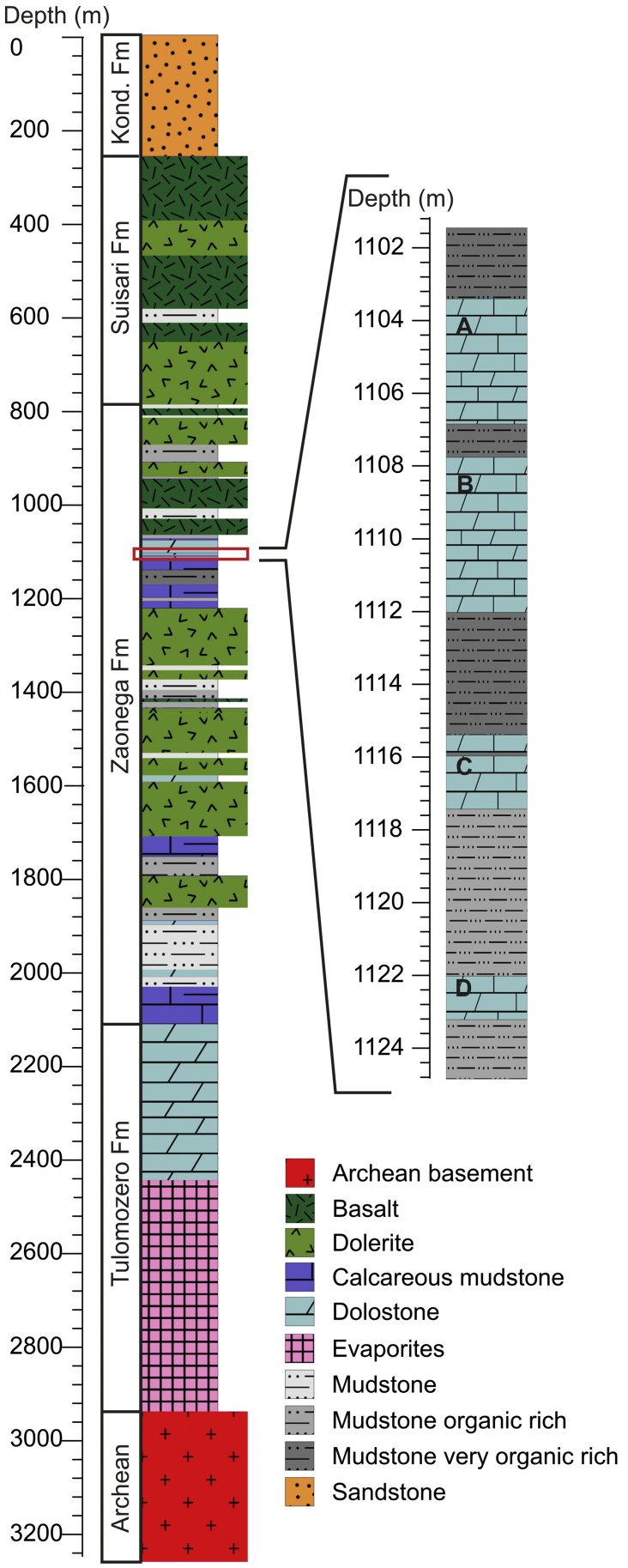
Depth (m)
0
200
400
600
800
1000
1200
1400
1600
1800
2000
2200
2400
2600
2800
3000
3200
Kond. Fm
Suisari Fm
Zaonega Fm
Tulomozero Fm
Archean
Depth (m)
1102
1104
1106
1108
1110
1112
1114
1116
1118
1120
1122
1124
A
B
C
D
Archean basement
Basalt
Dolerite
Calcareous mudstone
Dolostone
Evaporites
Mudstone
Mudstone organic rich
Mudstone very organic rich
Sandstone

Figure 2

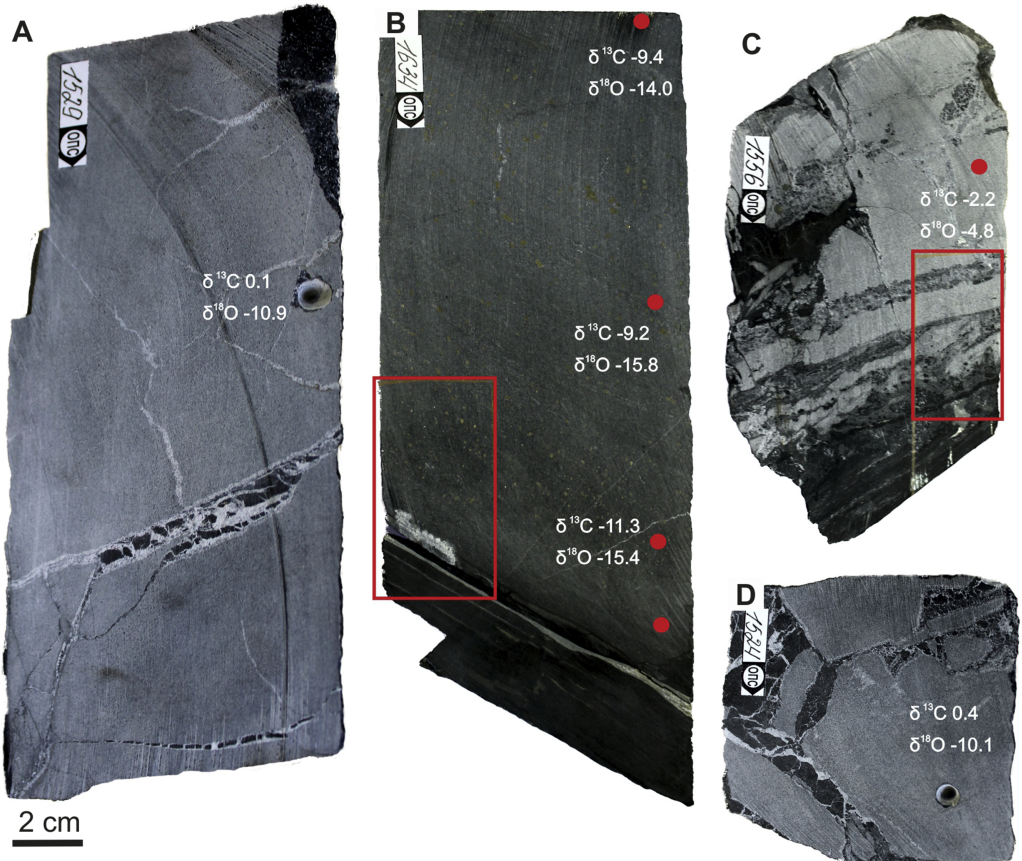
A
1539
δ13C 0.1
δ18O -10.9
B
1534
δ13C -9.4
δ18O -14.0
δ13C -9.2
δ18O -15.8
δ13C -11.3
δ18O -15.4
C
1536
δ13C -2.2
δ18O -4.8
D
1542
δ13C 0.4
δ18O -10.1
2 cm

Figure 3

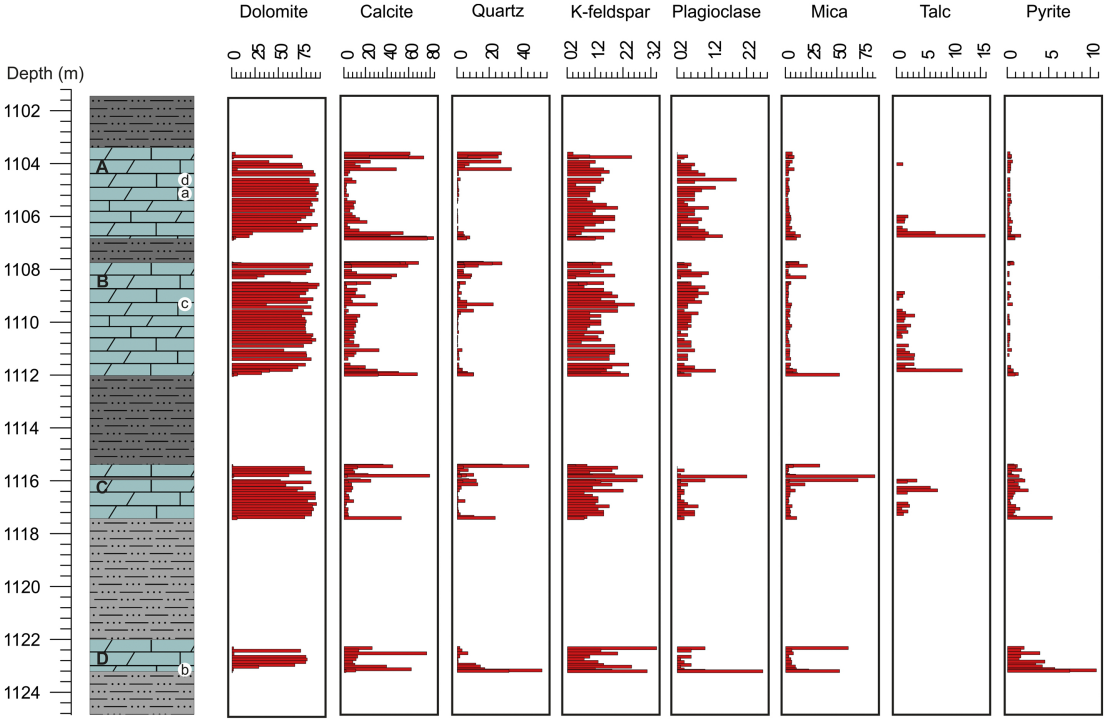
Depth (m)
1102
1104
1106
1108
1110
1112
1114
1116
1118
1120
1122
1124
A
B
C
D
a
b
c
d
Dolomite
0 25 50 75
Calcite
0 20 40 60 80
Quartz
0 20 40
K-feldspar
0.2 1.2 2.2 3.2
Plagioclase
0.2 1.2 2.2
Mica
0 25 50 75
Talc
0 5 10 15
Pyrite
0 5 10

Figure 4

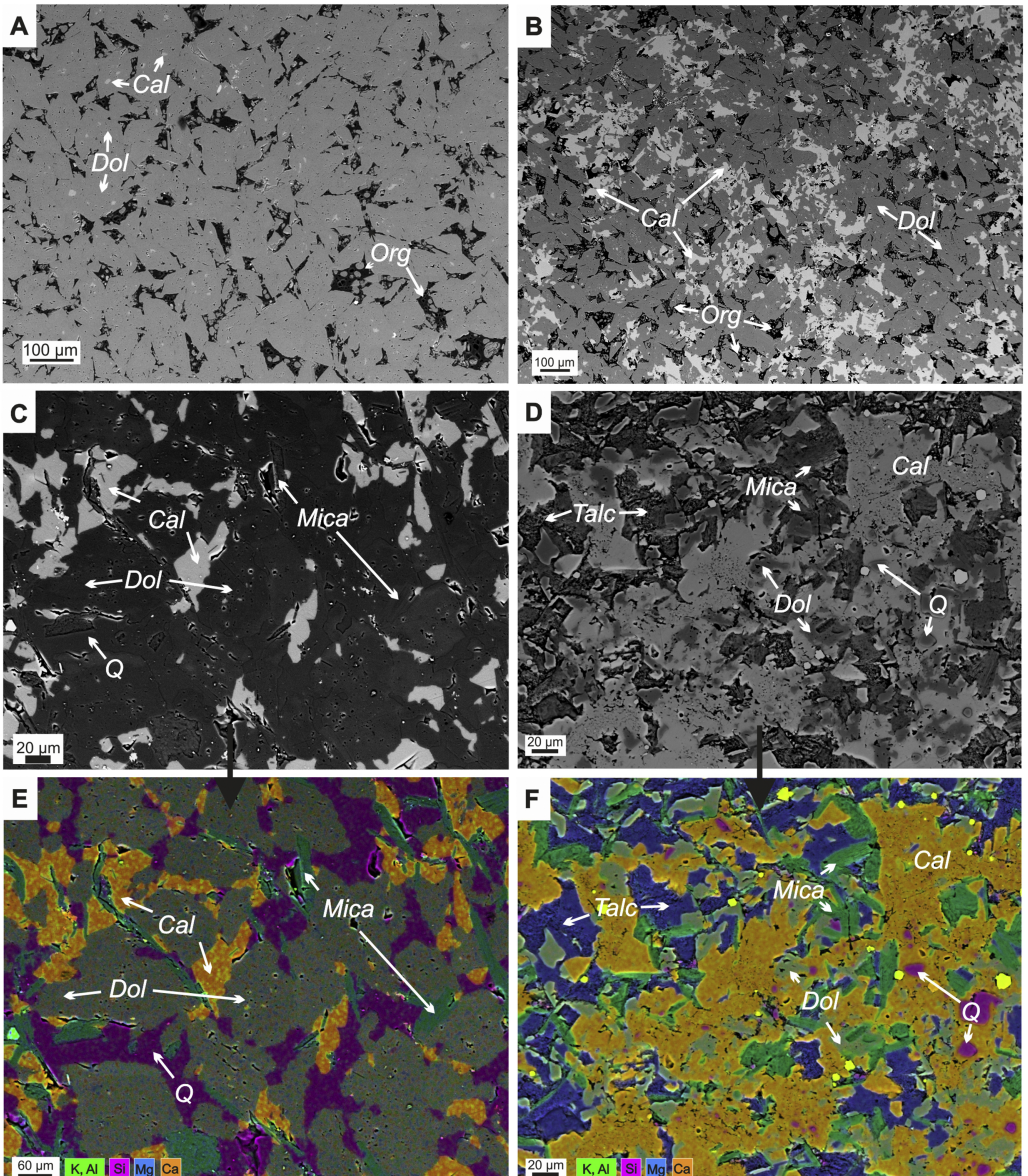
A
Cal
Dol
Org
100 µm
B
Cal
Dol
Org
100 µm
C
Cal
Mica
Dol
Q
20 µm
D
Cal
Mica
Talc
Dol
Q
20 µm
E
Cal
Mica
Dol
Q
60 µm
K, Al
Si
Mg
Ca
F
Cal
Mica
Talc
Dol
Q
20 µm
K, Al
Si
Mg
Ca

Figure 5

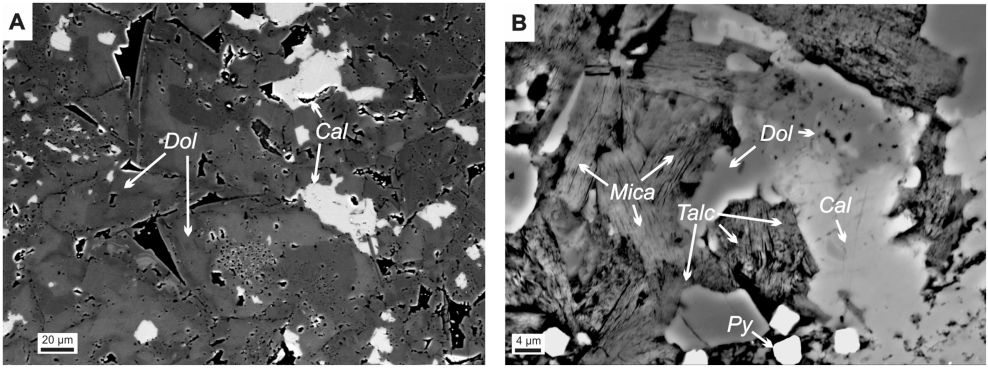

Figure 6

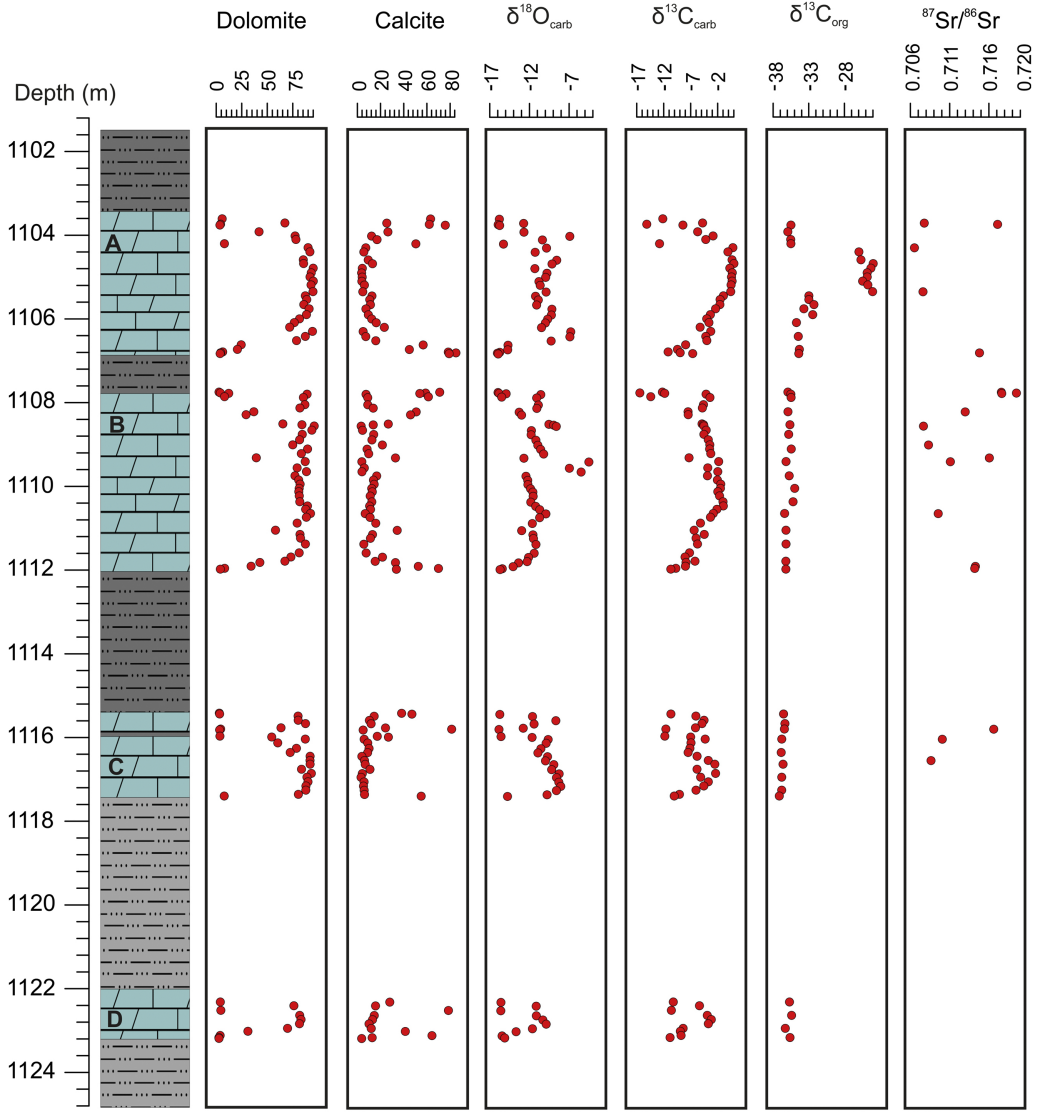
Depth (m)
1102
1104
1106
1108
1110
1112
1114
1116
1118
1120
1122
1124
A
B
C
D
Dolomite
0 25 50 75
Calcite
0 20 40 60 80
δ18Ocarb
-17 -12 -7
δ13Ccarb
-17 -12 -7 -2
δ13Corg
-38 -33 -28
87Sr/86Sr
0.706 0.711 0.716 0.720

Figure 7

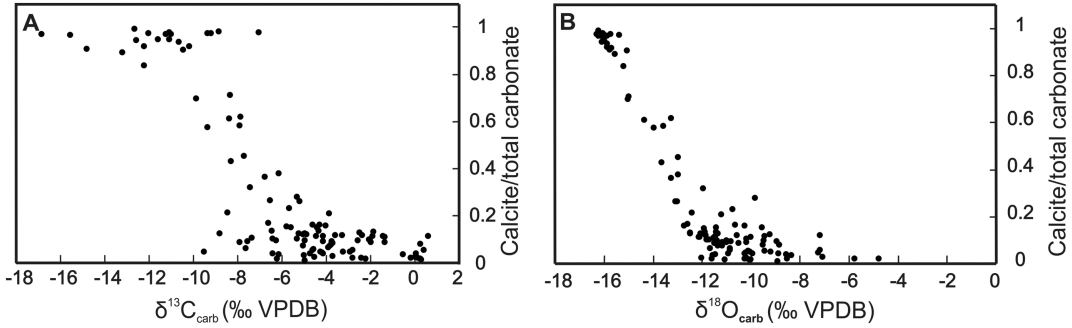
A
B
Calcite/total carbonate
1
0.8
0.6
0.4
0.2
0
-18
-16
-14
-12
-10
-8
-6
-4
-2
0
2
δ13Ccarb (‰ VPDB)
δ18Ocarb (‰ VPDB)

Figure 8

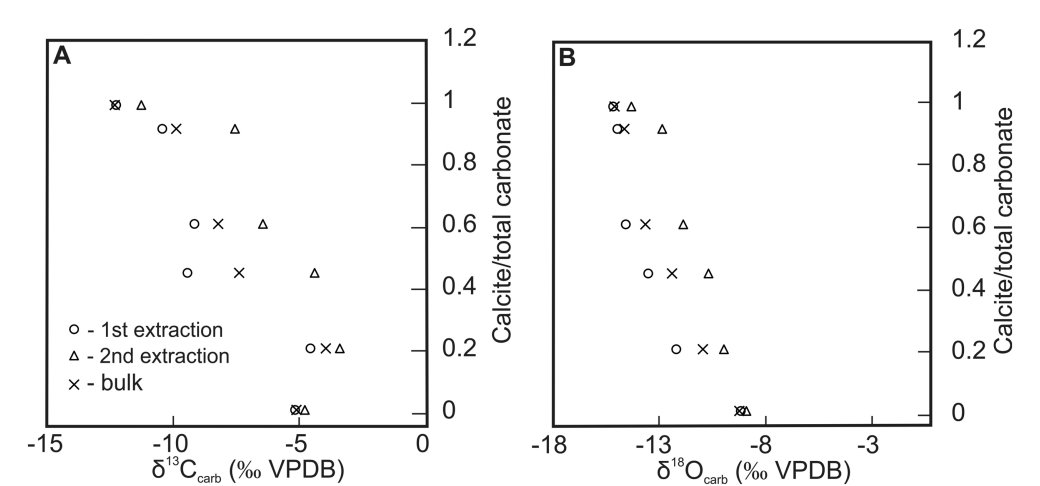
A
B
○ - 1st extraction
△ - 2nd extraction
× - bulk
Calcite/total carbonate
δ13Ccarb (‰ VPDB)
δ18Ocarb (‰ VPDB)
1.2
1
0.8
0.6
0.4
0.2
0
-15
-10
-5
0
-18
-13
-8
-3

Figure 9

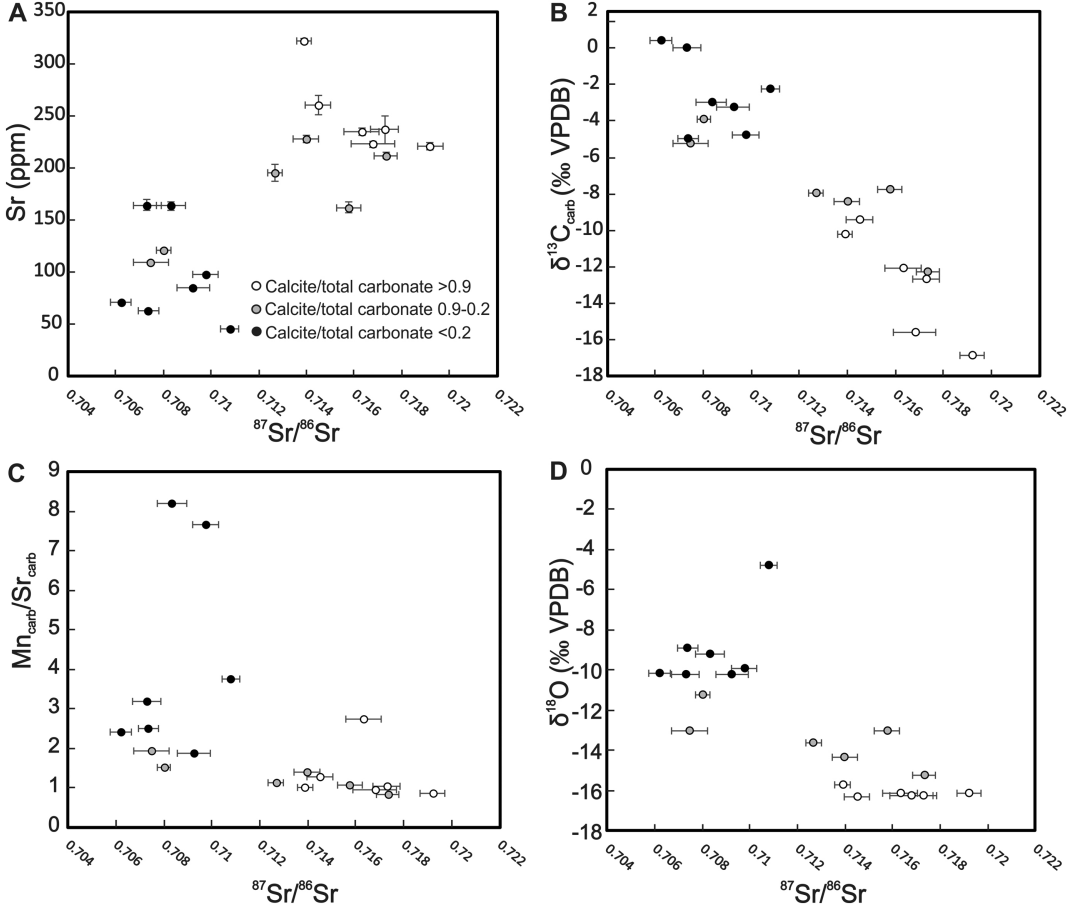
A
Sr (ppm)
$^{87}Sr/^{86}Sr$
Calcite/total carbonate >0.9
Calcite/total carbonate 0.9-0.2
Calcite/total carbonate <0.2
B
$\delta^{13}C_{carb}$ (‰ VPDB)
$^{87}Sr/^{86}Sr$
C
Mn_{carb}/Sr_{carb}
$^{87}Sr/^{86}Sr$
D
$\delta^{18}O$ (‰ VPDB)
$^{87}Sr/^{86}Sr$

Figure 10

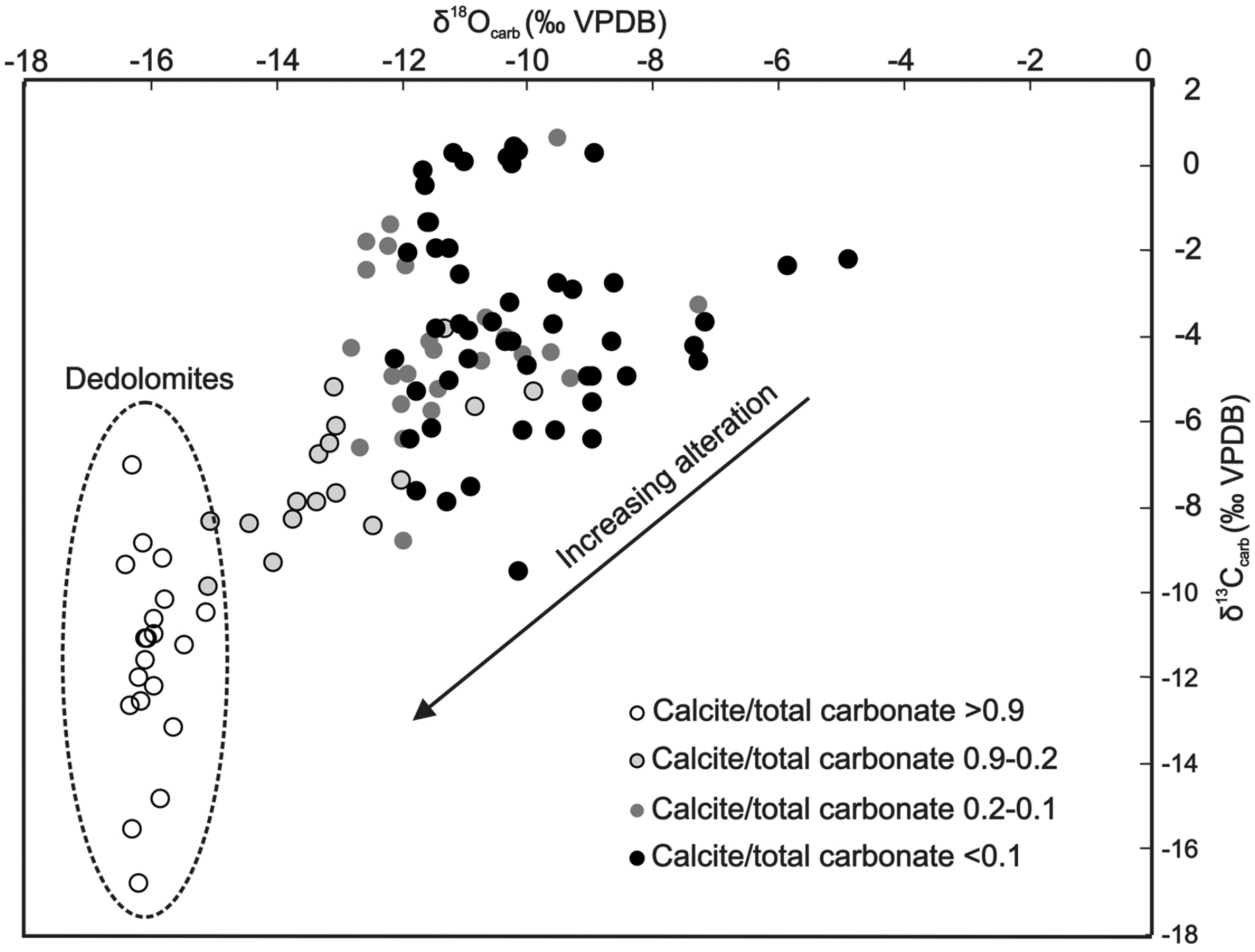
δ18Ocarb (‰ VPDB)
-18
-16
-14
-12
-10
-8
-6
-4
-2
0
2
0
-2
-4
-6
-8
-10
-12
-14
-16
-18
δ13Ccarb (‰ VPDB)
Dedolomites
Increasing alteration
Calcite/total carbonate >0.9
Calcite/total carbonate 0.9-0.2
Calcite/total carbonate 0.2-0.1
Calcite/total carbonate <0.1

Figure 11

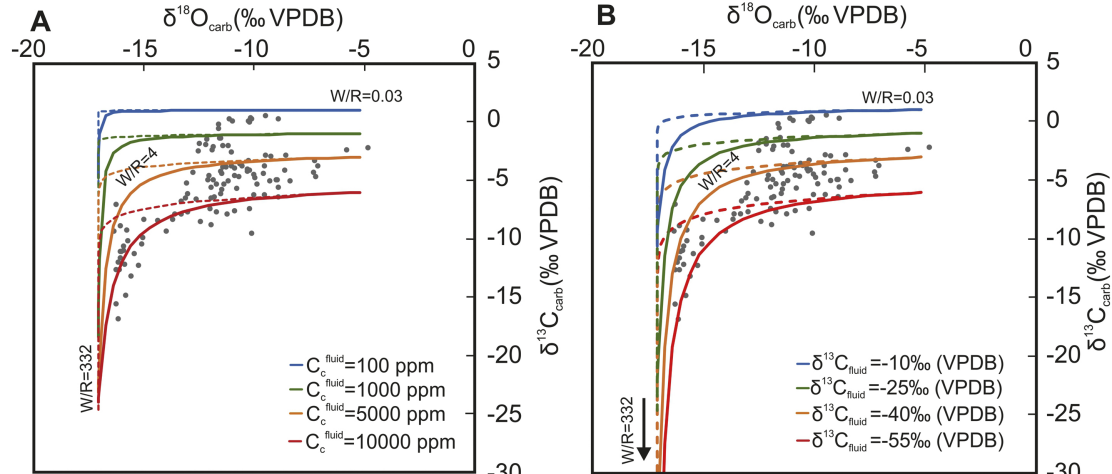
A
B
δ18Ocarb(‰ VPDB)
δ13Ccarb(‰ VPDB)
W/R=0.03
W/R=4
W/R=332
Cc fluid=100 ppm
Cc fluid=1000 ppm
Cc fluid=5000 ppm
Cc fluid=10000 ppm
δ13Cfluid=-10‰ (VPDB)
δ13Cfluid=-25‰ (VPDB)
δ13Cfluid=-40‰ (VPDB)
δ13Cfluid=-55‰ (VPDB)

Figure 12

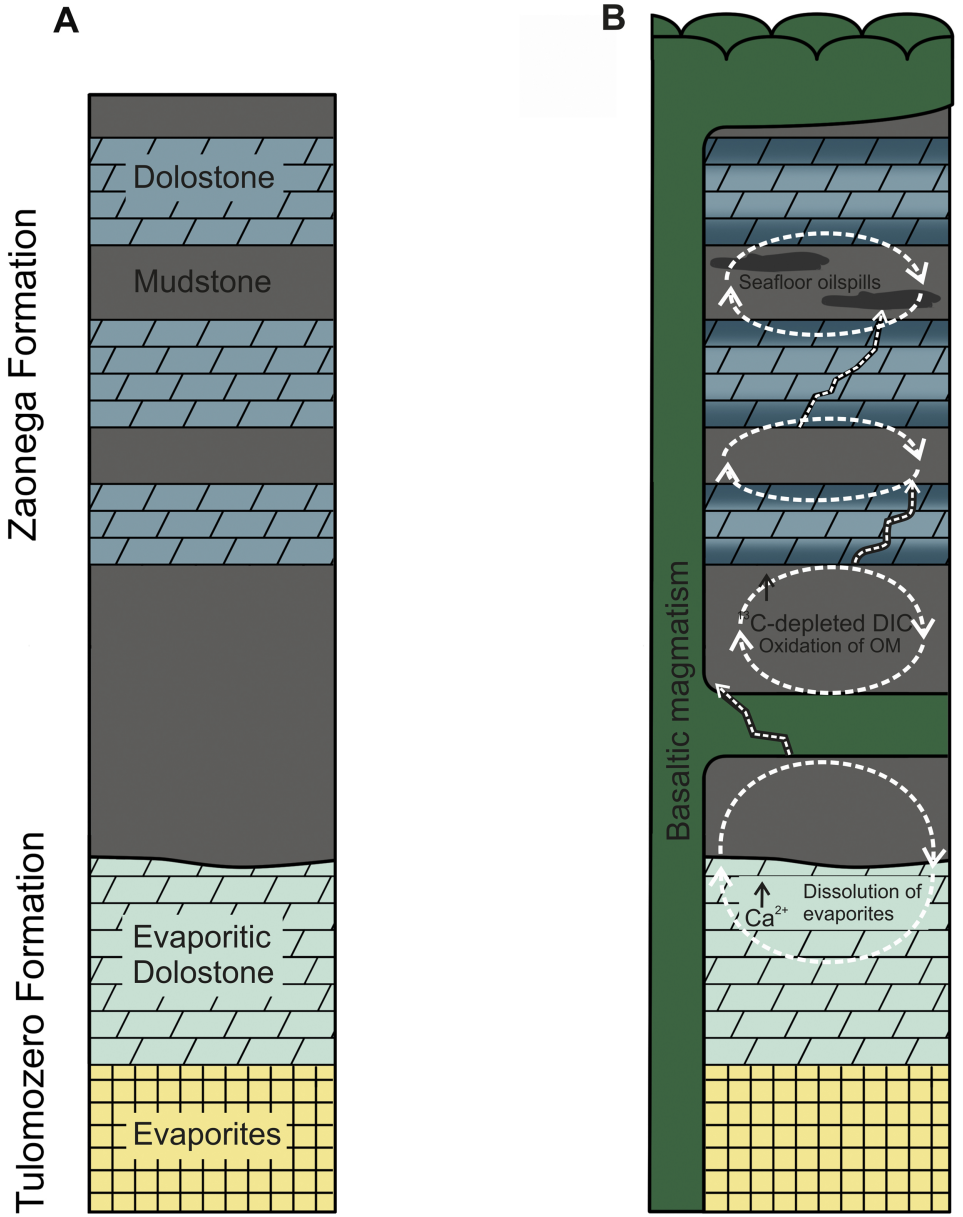
A
B
Zaonega Formation
Tulomozero Formation
Dolostone
Mudstone
Evaporitic Dolostone
Evaporites
Basaltic magmatism
Seafloor oilspills
C-depleted DIC
Oxidation of OM
Ca2+
Dissolution of evaporites

Figure 13

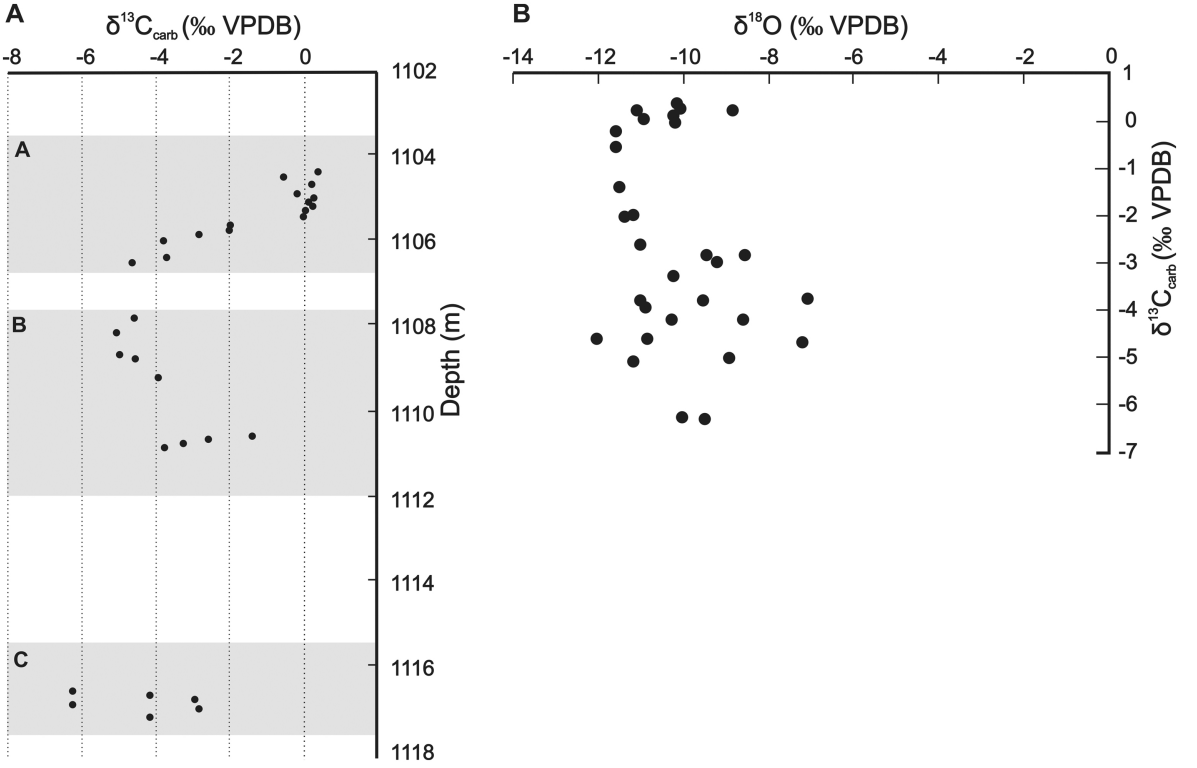
A
δ13Ccarb (‰ VPDB)
-8
-6
-4
-2
0
A
B
C
1102
1104
1106
1108
1110
1112
1114
1116
1118
Depth (m)
B
δ18O (‰ VPDB)
-14
-12
-10
-8
-6
-4
-2
0
1
0
-1
-2
-3
-4
-5
-6
-7
δ13Ccarb (‰ VPDB)

Figure 14